Article

THE EMBO JOURNAL

TECPR1 is activated by damage-induced sphingomyelin exposure to mediate noncanonical autophagy

Namrita Kaur[1,2] , Laura Rodriguez de la Ballina[1,3,†] , Håvard Styrkestad Haukaas[1,2,†] , Maria Lyngaas Torgersen[1,2], Maja Radulovic[1,2] , Michael J Munson[4] , Alan Sabirsh[4] , Harald Stenmark[1,2] , Anne Simonsen[1,2,3] , Sven R Carlsson[5] & Alf Håkon Lystad[1,2,3,*]

Abstract

Cells use noncanonical autophagy, also called conjugation of ATG8 to single membranes (CASM), to label damaged intracellular compartments with ubiquitin-like ATG8 family proteins in order to signal danger caused by pathogens or toxic compounds. CASM relies on E3 complexes to sense membrane damage, but so far, only the mechanism to activate ATG16L1-containing E3 complexes, associated with proton gradient loss, has been described. Here, we show that TECPR1-containing E3 complexes are key mediators of CASM in cells treated with a variety of pharmacological drugs, including clinically relevant nanoparticles, transfection reagents, antihistamines, lysosomotropic compounds, and detergents. Interestingly, TECPR1 retains E3 activity when ATG16L1 CASM activity is obstructed by the *Salmonella* Typhimurium pathogenicity factor SopF. Mechanistically, TECPR1 is recruited by damage-induced sphingomyelin (SM) exposure using two DysF domains, resulting in its activation and ATG8 lipidation. *In vitro* assays using purified human TECPR1-ATG5-ATG12 complex show direct activation of its E3 activity by SM, whereas SM has no effect on ATG16L1-ATG5-ATG12. We conclude that TECPR1 is a key activator of CASM downstream of SM exposure.

Introduction

The integrity of the cell's endolysosomal membranes can be compromised by many exogenous compounds, including cationic amphiphilic drugs, crystalline aggregates, and pathogens (Firestone *et al*, 1979; Yu *et al*, 2003; Shaughnessy *et al*, 2006; Mellouk *et al*, 2014; Flavin *et al*, 2017; Hou *et al*, 2021). Artificial delivery vehicles, such as lipid nanoparticles (LNPs) that are utilized for the delivery of mRNA therapeutics in COVID-19 vaccines (Jackson *et al*, 2020; Mulligan *et al*, 2020), also enter cells by endocytosis (Dowdy, 2017). These LNPs release their oligonucleotide cargo through endolysosomal damage/fusion events to achieve their therapeutic effect (Wittrup *et al*, 2015).

Our cells have developed various strategies to avoid leakage of ions and hydrolases into the cytosol upon endolysosomal damage, which potentially could activate cell death (Radulovic *et al*, 2018; Skowyra *et al*, 2018; Ellison *et al*, 2020; Zhen *et al*, 2021; Niekamp *et al*, 2022). Ca^{2+}-leakage and sphingomyelin (SM) exposure appear to be two crucial signals in the early host defense reaction. Another important feature is the rapid accumulation of phosphatidylinositol 4-phosphate (PtdIns4P) at the site of damage, where it plays a role in the recruitment of repair proteins and establishment of contacts between the endoplasmic reticulum (ER) and the damaged lysosome (Radulovic *et al*, 2022; Tan & Finkel, 2022). If the early response to lysosome damage fails, canonical autophagy activates to engulf the whole organelle (lysophagy), triggered by exposure of luminal glycans that are recognized by galectins in a ubiquitin-dependent process (Maejima *et al*, 2013).

A hallmark of autophagy is the conjugation of ATG8 family proteins (LC3 and GABARAP subfamilies) to phosphatidylethanolamine (PE) in the autophagic membrane, a process coined ATG8ylation (Kumar *et al*, 2021). The main role of ATG8 on these membranes is to bind proteins containing an LC3 interacting region (LIR),

1 Centre for Cancer Cell Reprogramming, Faculty of Medicine, University of Oslo, Oslo, Norway
2 Department of Molecular Cell Biology, Institute for Cancer Research, Oslo University Hospital, Oslo, Norway
3 Department of Molecular Medicine, Institute of Basic Medical Sciences, University of Oslo, Oslo, Norway
4 Advanced Drug Delivery, Pharmaceutical Sciences, Biopharmaceuticals R&D, AstraZeneca, Gothenburg, Sweden
5 Department of Medical Biochemistry and Biophysics, University of Umeå, Umeå, Sweden
*Corresponding author. Tel: +47 22781822; E-mail: alfly@medisin.uio.no
†These authors contributed equally to this work

including receptors for cargo to be degraded, but also proteins involved in phagophore elongation and autophagosome closure, transport, tethering, and fusion with other membranes (Maruyama & Noda, 2021). The consecutive steps of the conjugation reaction are well established, proceeding through E1, E2, and E3 reactions, similar to ubiquitination. The E1 enzyme ATG7 activates and delivers ATG8 to the E2 enzyme ATG3, which in turn conjugates ATG8 to PE in concert with the E3 complex ATG16L1-ATG5-ATG12 (Mizushima, 2020). ATG16L1 recognizes the target membrane to ensure that the ATG8 lipidation reaction occurs at the correct site (Fujita *et al*, 2008).

In recent years, we have learned that the ATG8/LC3 conjugation machinery is also involved in autophagy-independent events, referred to as noncanonical autophagy or conjugation of ATG8 to single membranes (CASM) (Durgan *et al*, 2021). This process requires ATG16L1 and the Vacuolar type ATPase (V-ATPase) and also includes the conjugation of ATG8 to phosphatidylserine (PS) (Fletcher *et al*, 2018; Xu *et al*, 2019; Durgan *et al*, 2021; Hooper *et al*, 2022). The V-ATPase senses the loss of a proton gradient and signals ATG16L1 to initiate ATG8 lipidation directly on the compromised membrane (Hooper *et al*, 2022). This mechanism is believed to sense harmful agents, like pathogens, taken up in the endolysosomal system and thereby provide protection. Indeed, certain pathogens specifically block CASM to thrive within compartments of the host. For instance, *Legionella pneumophila* uses RavZ to terminally destroy the ATG8 proteins of the host (Choy *et al*, 2012) while the *Salmonella* Typhimurium protein SopF blocks the interaction between ATG16L1 and the V-ATPase to abolish CASM (Xu *et al*, 2019).

In both canonical and noncanonical autophagy, membrane targeting of the E3 complex is mediated by ATG16L1 (Fujita *et al*, 2008; Hooper *et al*, 2022). Possibly in order to increase the repertoire of potential ATG8ylation events, vertebrates have developed two alternative complex partners for ATG5-ATG12, namely ATG16L2 and Tectonin Beta-Propeller Repeat Containing 1 (TECPR1). ATG16L2 is similar to ATG16L1 in sequence and domain organization but cannot replace ATG16L1 in canonical autophagy (Ishibashi *et al*, 2011), and its function is so far unknown. TECPR1 has a completely different domain organization, consisting of two tectonin 6-bladed propellers, each having an integrated Dysferlin (DysF) domain, together with a pleckstrin homology (PH) domain

between the propellers (Ogawa *et al*, 2011; Chen *et al*, 2012; Wetzel *et al*, 2020). The three variants (ATG16L1, ATG16L2 and TECPR1) share the ability to form stable complexes with ATG5-ATG12, and they do so through a common ATG5-binding α-helix (AIM, ATG5-interacting motif) (Kim & Song, 2015), which in the case of TECPR1 is located just upstream of the PH domain.

Here we show that the TECPR1-ATG5-ATG12 complex recognizes SM exposed on endolysosomal membranes in response to diverse insults, leading to ATG8ylation of the damaged membrane in a novel form of CASM.

Results

TECPR1 mediates ATG16L1-independent ATG8ylation in response to endolysosomal insults

Previous studies have shown that ATG16L1 specifies the site of lipidation of ATG8 proteins of the LC3 and GABARAP subfamilies (Fujita *et al*, 2008), and that ATG16L1-knockout (KO) cells are devoid of lipid-conjugated LC3/GABARAP upon induction of autophagy or CASM (Fletcher *et al*, 2018; Lystad *et al*, 2019). We were therefore surprised to find that certain agents that cause damage to endolysosomal compartments, including nanoparticles containing the clinically relevant cationic lipid dilinoleylmethyl-4-dimethylamino-butyrate (DLin-MC3-DMA, hereafter referred to as MC3) used in the siRNA drug Patisiran (Akinc *et al*, 2019) and a lysosomotropic agent (L-leucyl-L-leucine methyl ester, LLOMe), caused ATG8ylation (LC3B and GABARAP lipidation) even in ATG16L1-KO HEK293A cells (Fig 1A and B). Intriguingly, MC3- and LLOMe-induced ATG16L1-independent ATG8ylation showed an absolute requirement for ATG5 (Fig 1C and D), implying that an alternative ATG5-containing E3 complex might facilitate membrane targeting of the conjugation machinery during such conditions. We therefore tested different single, double, and triple KO combinations of ATG16L1, ATG16L2, and TECPR1 in PC-3 cells, all known ATG5 interactors, to determine whether ATG16L2 or TECPR1 could substitute for ATG16L1-mediated ATG8ylation in cells treated with MC3 or LLOMe (Fig 1E). As CASM occurs independently of the ULK and VPS34 complexes, cells were co-treated with the ULK inhibitor MRT68921 and the VPS34 inhibitor SAR405 to reduce background

---

Figure 1. TECPR1 facilitates ATG16L1-independent ATG8ylation.

A   Immunoblot analysis of LC3B and GABARAP lipidation in wild-type (WT) and ATG16L1-KO HEK293A cells, with or without stimulation for 2 h as indicated. BafA1 stands for Bafilomycin A1. Gamma-Tubulin (γ-Tubulin) is a loading control.

B   Densitometry analysis of lipidated LC3B (LC3B-II) to γ-tubulin (normalized to untreated WT cells) from immunoblots in (A).

C   LC3B/GABARAP lipidation in ATG16L1- and ATG5-KO HEK293A cells treated for 2 h as indicated. Vinculin is a loading control. Cell lysates were immunoblotted for the specified proteins.

D   Ratio of LC3B-II to Vinculin quantified from immunoblots in (C) and normalized to MC3 treated ATG16L1 KO cells.

E   Immunoblot analysis of LC3B and GABARAP lipidation from WT, ATG16L1-KO (L1-KO), ATG16L2-KO (L2-KO), TECPR1-KO (TECKO), ATG16L1/L2-DKO (L1/L2-DKO), ATG16L1/TECPR1-DKO (L1/TEC DKO), and ATG16L1/L2/TECPR1-TKO (L1/L2/TEC-TKO) PC-3 cells, treated as indicated for 2 h, were immunoblotted for the indicated proteins. Vinculin is a loading control. MRT68921 and SAR405 are ULK and VPS34 inhibitors, respectively.

F   Ratio of LC3B-II to Vinculin quantified from immunoblots in (E) and normalized to MC3 treated WT cells.

G   LC3B/GABARAP lipidation in ATG16L1-KO and ATG16L1/TECPR1-DKO HEK293A cells with or without TECPR1 rescue, treated as indicated for 2 h. Cell lysates were immunoblotted against the indicated proteins. Vinculin is a loading control.

H   Ratio of LC3B-II to Vinculin quantified from immunoblots in (G) and normalized to ATG16L1-KO cells treated with MC3.

Data information: All data presented as mean + SEM, from *n* = 3 independent experiments. *P*-value determined using two-way ANOVA followed by the Tukey's multiple comparisons test; ns = not significant.
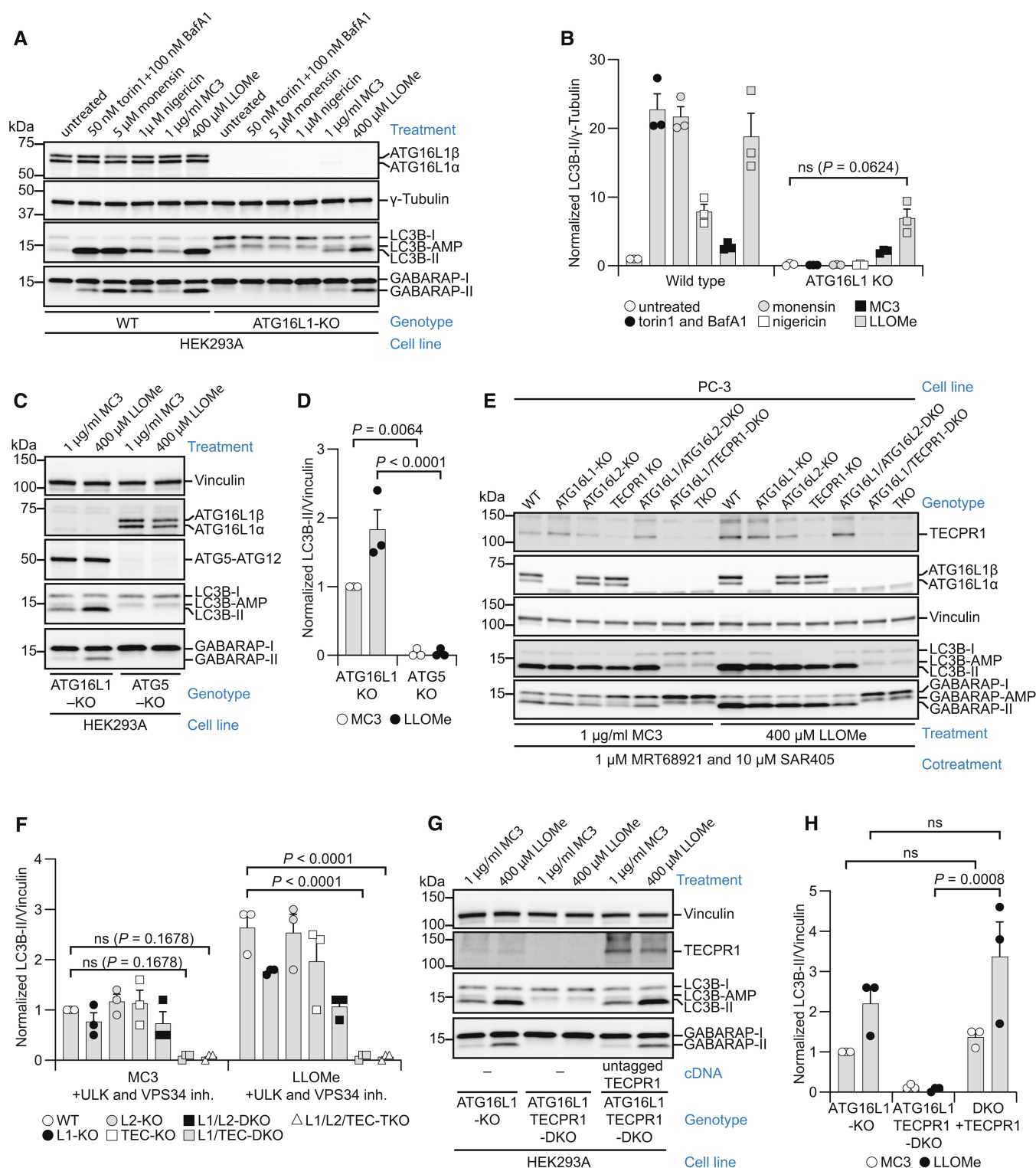
Figure 1.

LC3B lipidation caused by canonical macroautophagy. Depletion of ATG16L2 had no significant effect on LC3B/GABARAP lipidation in any of the combinations. Interestingly, co-depletion of ATG16L1 and TECPR1 completely prevented LC3B/GABARAP lipidation

(Fig 1E and F) in cells treated with MC3 or LLOMe, suggesting that these two E3 proteins function redundantly under these conditions. This result further highlighted that TECPR1-mediated CASM is independent of ULK and VPS34 activity. Importantly, we could restore

the defective lipidation activity in ATG16L1/TECPR1-double KO (DKO) cells by reintroducing TECPR1 using lentiviral transduction (Fig 1G and H), showing that TECPR1 is sufficient for ATG8ylation.

To further identify conditions under which TECPR1 might promote ATG8ylation, HEK293A cells (wild-type (WT), ATG16L1-KO, ATG16L1/TECPR1-DKO and ATG16L1/TECPR1-DKO with TECPR1 rescue) were treated with a variety of compounds that have been shown to affect endolysosomal membranes (Fig EV1). TECPR1 activity was required for ATG8ylation in cells lacking ATG16L1 when treated with the detergent saponin, the transfection reagent JetMESSENGER®, the cathepsin C substrate glycyl-L-phenylalanine 2-naphththylamide (GPN) and the cationic amphiphilic antihistamine astemizole, but not for ATG8ylation in response to ammonium chloride (NH₄Cl), the autophagy inducer torin1, or the ionophores monensin and nigericin (Fig EV1). This indicates that the activity of TECPR1 is induced by drugs that affect endolysosomal membrane integrity but not by drugs that affect autophagy or the endolysosomal proton gradient.

To determine whether TECPR1 is recruited to endolysosomal membranes in a similar manner as ATG16L1, which interacts with the V-ATPase (Xu *et al*, 2019), we isolated V-ATPases from HEK293A cells treated with LLOMe using a bait of N-terminally EGFP-tagged SidK, a *Legionella pneumophila* effector protein shown to bind V-ATPases with high affinity (Abbas *et al*, 2020). Immunoblotting of the immunoprecipitates showed that while ATG16L1 clearly interacts with the EGFP-SidK-V-ATPase complex, TECPR1 did not, suggesting that it is recruited through a different mechanism than ATG16L1 (Fig EV2A–C).

Together, our data clearly show that TECPR1 participates in a functional E3 complex that facilitates the lipidation of LC3B and GABARAP proteins under specific stressors independently of ATG16L1.

TECPR1 is a sensor for compromised compartments

To gain further insight into the function of TECPR1, we generated HeLa cells lacking both ATG16L1 and TECPR1 (DKO cells) that were rescued with EGFP-tagged TECPR1. Due to challenges we encountered during immunoblotting for endogenous TECPR1 in these HeLa cells, we utilized Sanger sequencing to identify the indels produced by CRISPR/Cas9 (Appendix Fig S1).

As for HEK293A cells, EGFP-TECPR1 fully rescued ATG8ylation upon LLOMe treatment (Fig 2A and B), showing that the role of TECPR1 in ATG8ylation is not cell-type-specific. Furthermore, we observed that, similar to HEK293A cells, TECPR1 in HeLa cells was

not activated by torin1 or monensin (Fig 2A and B), emphasizing that membrane damage is a prerequisite for TECPR1 activation. By contrast, cells expressing EGFP-ATG16L1β showed WT-like levels of ATG8ylation not only in response to LLOMe but also to torin1 and monensin (Fig 2A and B).

Importantly, diverse cell lines display variations in their TECPR1 response when confronted with membrane damage, as illustrated by the varying degrees of TECPR1-dependent ATG8 lipidation in HEK293A (Fig 1A and B), PC-3 (Fig 1E and D), and HeLa (Fig 2A and B) cells. Such cell line-specific variation may provide an explanation for the near-complete ATG16L1-dependence observed in previous studies that examined ATG8 lipidation in response to membrane-damaging agents (Nakamura *et al*, 2020; preprint: Cross *et al*, 2023).

To investigate the subcellular localization of TECPR1, we introduced mScarlet-LC3B to the DKO cells expressing EGFP-TECPR1. Upon treatment with Cy5-labeled MC3 lipid nanoparticles, both EGFP-TECPR1 and mScarlet-LC3B were recruited to the Cy5-positive structures (Fig 2C). By contrast, translocation of LC3B to nanoparticle-containing structures did not occur in the DKO cells lacking EGFP-TECPR1, showing that TECPR1 is required for targeting LC3B to the damaged membrane. Puncta recruitment of EGFP-TECPR1 and mScarlet-LC3B was also observed in cells treated with LLOMe (Fig 2C). By using live-cell imaging, we found that EGFP-TECPR1 and mScarlet-LC3B assembled into puncta within 1–5 min of LLOMe treatment (Fig 2D). This is in line with immunoblot data from ATG16L1-KO HEK293A cells where LC3/GABARAP lipidation had already begun 5 min after the addition of LLOMe (Fig 2E and F). Note that disruption of autophagy with ATG16L1-KO causes the formation of SQSTM1 bodies that act as sinks for unlipidated LC3 (LC3-I), which are visible as aggregate-like structures in such cells (Runwal *et al*, 2019; Fig EV3C). Further analyses of the TECPR1 puncta induced by LLOMe and MC3 treatment showed that they overlapped with LAMP1 and were positive for Ubiquitin, SQSTM1, and Galectin-3, while no such overlap could be seen in the untreated condition (Fig EV3A–F). Treatment with MC3 also resulted in the partial overlap between TECPR1 and EEA1, an early endosomal marker, suggesting that TECPR1 is not restricted to lysosomal compartments (Fig EV3G). Upon inducing membrane damage with LLOMe, we also confirm a high degree of overlap between EGFP-TECPR1 and mCherry-ATG16L1β induced puncta (Fig EV3H). Taken together, we conclude that TECPR1 is recruited together with LC3B to damaged compartments of the endolysosomal system, where TECPR1 facilitates LC3B and GABARAP lipidation.

Figure 2. TECPR1 is a sensor for compromised compartments.

A LC3B/GABARAP lipidation in WT, ATG16L1/TECPR1-DKO HeLa cells with and without EGFP-TECPR1 or EGFP-ATG16L1β rescue, treated for 2 h as indicated. Cell lysates were immunoblotted for the indicated proteins. γ-Tubulin is a loading control.

B Ratio of LC3B-II to γ-Tubulin quantified from immunoblots in (A) and normalized to untreated WT cells (Data presented as mean + SEM, $n = 3$ independent experiments, *P*-value from two-way ANOVA followed by Tukey's multiple comparisons test; ns = not significant).

C Confocal images of ATG16L1/TECPR1-DKO HeLa cells expressing mScarlet-LC3B, with or without EGFP-TECPR1, treated for 2 h with Cy5-labeled MC3 particles (left) or LLOMe (right) as indicated. Scale bars: 10 μm.

D Confocal time-lapse images of ATG16L1/TECPR1-DKO HeLa cells, showing localization of mScarlet-LC3B and EGFP-TECPR1, after treatment with 400 μM LLOMe. Scale bar: 10 μm.

E Immunoblot analysis of LC3B/GABARAP lipidation in ATG16L1-KO HEK293A cells, treated with 400 μM LLOMe for indicated periods. γ-Tubulin is a loading control.

F Ratio of LC3B-II to γ-Tubulin quantified from immunoblots in (E) and normalized to 2 h (120 min) LLOMe treatment (Data presented as mean + SEM, $n = 4$ independent experiments, *P*-value from two-way ANOVA followed by Tukey's multiple comparisons test).
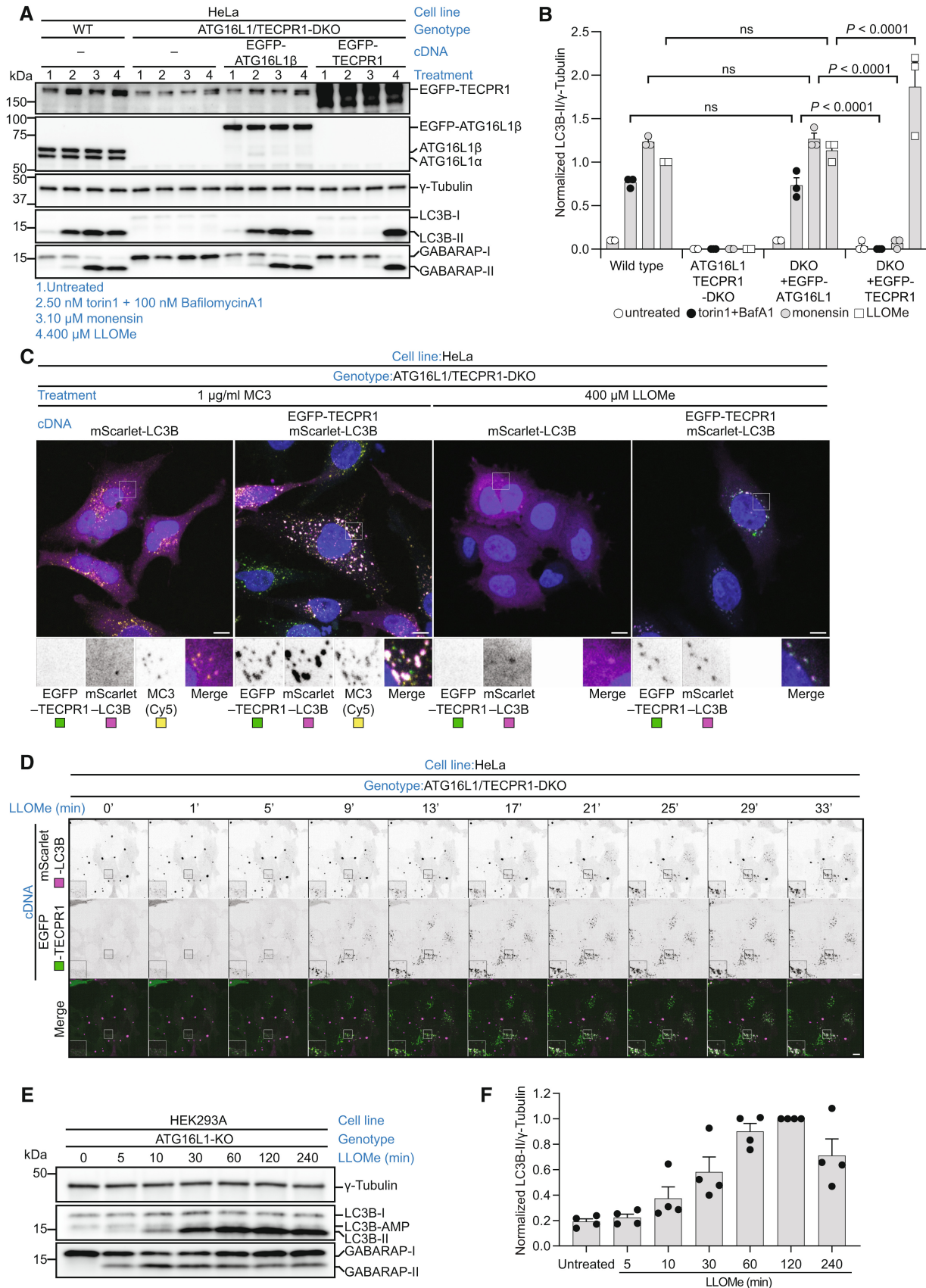
Figure 2.

Sphingomyelin, found on damaged endolysosomes, is a key inducer of TECPR1 E3-activity

Recent reports show that SM is presented on the cytosolic leaflet of lysosomal compartments following LLOMe treatment (Ellison *et al*, 2020; Niekamp *et al*, 2022). We therefore wanted to explore the possible role of SM in TECPR1 activation. To this end, we established HeLa ATG16L1/TECPR1-DKO cells co-expressing EGFP-TECPR1 and EqtSM-mCherry, a probe based on the pore-forming toxin equinatoxin II that specifically detects SM exposed on the cytosol-facing lipid leaflet of intracellular compartments (Niekamp *et al*, 2022). Using this cell line, we observed by live-cell imaging that SM exposure to the cytosol coincides with TECPR1 recruitment upon LLOMe treatment (Fig 3A).

To investigate the role of SM in TECPR1 recruitment, HEK293A cells lacking TECPR1 or ATG16L1 were transfected with nSMase2-mCherry to deplete SM exposed upon LLOMe treatment. Interestingly, nSMase2-mCherry overexpression abolished TECPR1 E3-activity in LLOMe-treated ATG16L1 KO cells, while having no effect on ATG16L1 activity in TECPR1 KO cells (Fig 3B and C). Furthermore, complementing ATG16L1/TECPR1-DKO HeLa cells expressing EGFP-TECPR1 with nSMase2 led to a deficiency in LC3 lipidation and disrupted EGFP-TECPR1 recruitment into puncta, providing further evidence for the role of SM in TECPR1 activation (Fig 3D–F).

Having confirmed that TECPR1 becomes recruited to SM-positive structures in response to lysosomal damage, we addressed whether SM might directly affect TECPR1-mediated LC3B lipidation. For this purpose, purified proteins, namely ATG7 (E1), ATG3 (E2), and ATG16L1-ATG5–ATG12 (E3) or TECPR1-ATG5–ATG12 (E3), were incubated with liposomes to reconstitute lipidation of purified LC3B *in vitro* as described previously (Lystad *et al*, 2019). Intriguingly, while SM in liposomes had no effect on LC3B lipidation facilitated by the ATG16L1-containing E3 complex, SM was essential for efficient LC3B lipidation reactions using a TECPR1-containing E3 complex (Fig 3G and H). This shows a striking difference between the two E3 complexes and clearly demonstrates the importance of SM for TECPR1-mediated LC3B lipidation but not for ATG16L1 activity.

In order to gain a deeper understanding of the E3 activity of TECPR1, we performed *in vitro* lipidation experiments using all six ATG8 proteins (LC3A, LC3B, LC3C, GABARAP, GABARAPL1, and GABARAPL2). We also explored the potential of PS to act as a substrate for ATG8 conjugation facilitated by TECPR1 *in vitro*. Our findings revealed that TECPR1 can facilitate the conjugation of all ATG8 proteins, and that this process is SM-specific (Fig EV4A–E). In addition, we discovered that TECPR1 enables the use of PS as a substrate for ATG8ylation *in vitro*, albeit at lower lipidation rates (Fig EV4D and E). Interestingly, we observed a noteworthy synergistic effect in the lipidation process when both PE and PS were present (Fig EV4D and E).

The SM-dependent activation of TECPR1 suggested that TECPR1 might interact directly with SM, and we therefore set out to identify possible SM-recognizing regions of TECPR1. To this end, we made several attempts to purify the TECPR1-ATG5-ATG12 complex with truncations in various regions of the protein. In most cases, the protein complex became unstable and was not suited for testing in lipidation and liposome binding assays. However, the removal of the DysF domains, both as single and double deletions yielded stable material suited for *in vitro* analyses. Analysis of their membrane-binding activity by liposome co-sedimentation revealed that while full-length (FL) TECPR1 binds to liposomes containing SM, binding was considerably reduced with SM-free liposomes, confirming its interaction with SM (Fig 3I and J). Interestingly, membrane binding of TECPR1 lacking both DysF domains was significantly reduced compared with FL TECPR1, indicating that these domains are sensors for SM (Fig 3I and J).

It was recently shown that PtdIns4P accumulates on damaged lysosomes through the activity of phosphatidylinositol 4-kinase type 2α (PI4K2A). However, although PI4K2A-KO HeLa cells (Fig EV5A) stably expressing mNeonGreen-TECPR1 were disrupted in recruitment of the PtdIns4P probe mCherry-2XSidM compared with WT

Figure 3. Sphingomyelin, found on damaged endolysosomes, is a key inducer of TECPR1 E3-activity.

A Time series of confocal images showing redistribution of EqtSM-mCherry (sphingomyelin (SM) probe) and EGFP-TECPR1 in ATG16L1/TECPR1-DKO cells with doxycycline-inducible (dox, 2 μg/ml) expression of EqtSM-mCherry cells following treatment with 400 μM LLOMe. Scale bar: 10 μm.

B LC3B/GABARAP lipidation in ATG16L1- and TECPR1-KO HEK293A cells with or without dox-inducible (2 μg/ml) expression of nSMase2-mCherry, treated for 2 h as indicated. Cell lysates were immunoblotted against the indicated proteins. γ-Tubulin is a loading control.

C Ratio of LC3B-II to γ-Tubulin quantified from immunoblots in (B) and normalized to untreated ATG16L1-KO cells (Data presented as mean + SEM, *n* = 3 independent experiments, *P*-value from two-way ANOVA followed by Tukey's multiple comparisons test; ns = not significant).

D LC3B/GABARAP lipidation in ATG16L1/TECPR1-DKO HeLa cells with or without dox-inducible (2 μg/ml) expression of untagged-nSMase2, treated for 2 h as indicated. Cell lysates were immunoblotted against the indicated proteins. γ-Tubulin is a loading control.

E Confocal images of ATG16L1/TECPR1-DKO HeLa cells expressing EGFP-TECPR1, with or without dox-inducible (2 μg/ml) nSMase2 overexpression, treated for 2 h as indicated. Scale bars: 10 μm.

F Beeswarm-Superplot displaying the mean number of EGFP-TECPR1 dots per cell per image of data represented in (E) quantified by automated analysis using CellProfiler. Mean ± SEM from each independent experiment (3/group) presented as large data points, with the black line corresponding to the mean of means. Individual data points (small) corresponding to single images are color-coded and superimposed according to the biological replicate they originate from. Total cells per condition/images per condition: 952/30 (LLOMe treated − nSMase2) and 1056/30 (LLOMe treated + nSMase2) were analyzed (*P*-values determined using Student's unpaired *t*-test).

G Coomassie-stained gel depicting *in vitro* LC3B lipidation reactions using the indicated combinations of proteins and liposomes (with or without SM), after being subjected to a liposome co-sedimentation assay. Separation of reactions into membrane bound (pellet) and supernatant allows clear distinction of LC3B-II and LC3B-AMP. LC3B-AMP is denoted with an asterisk (*).

H The extent of LC3B-I to -II conversion in (G) was determined and plotted as percentage of total LC3B (Data presented as mean + SEM, *n* = 3 independent experiments, *P*-value from two-way ANOVA followed by Tukey's multiple comparisons test; ns = not significant).

I Liposome co-sedimentation assay of the indicated recombinant proteins and liposomes with or without SM. S: supernatant; P: pellet.

J Liposome binding in (C) was quantified as percentage of total protein in the pellet (Data presented as mean + SEM, *n* = 3 independent experiments, *P*-value from two-way ANOVA followed by Tukey's multiple comparisons test; ns = not significant).
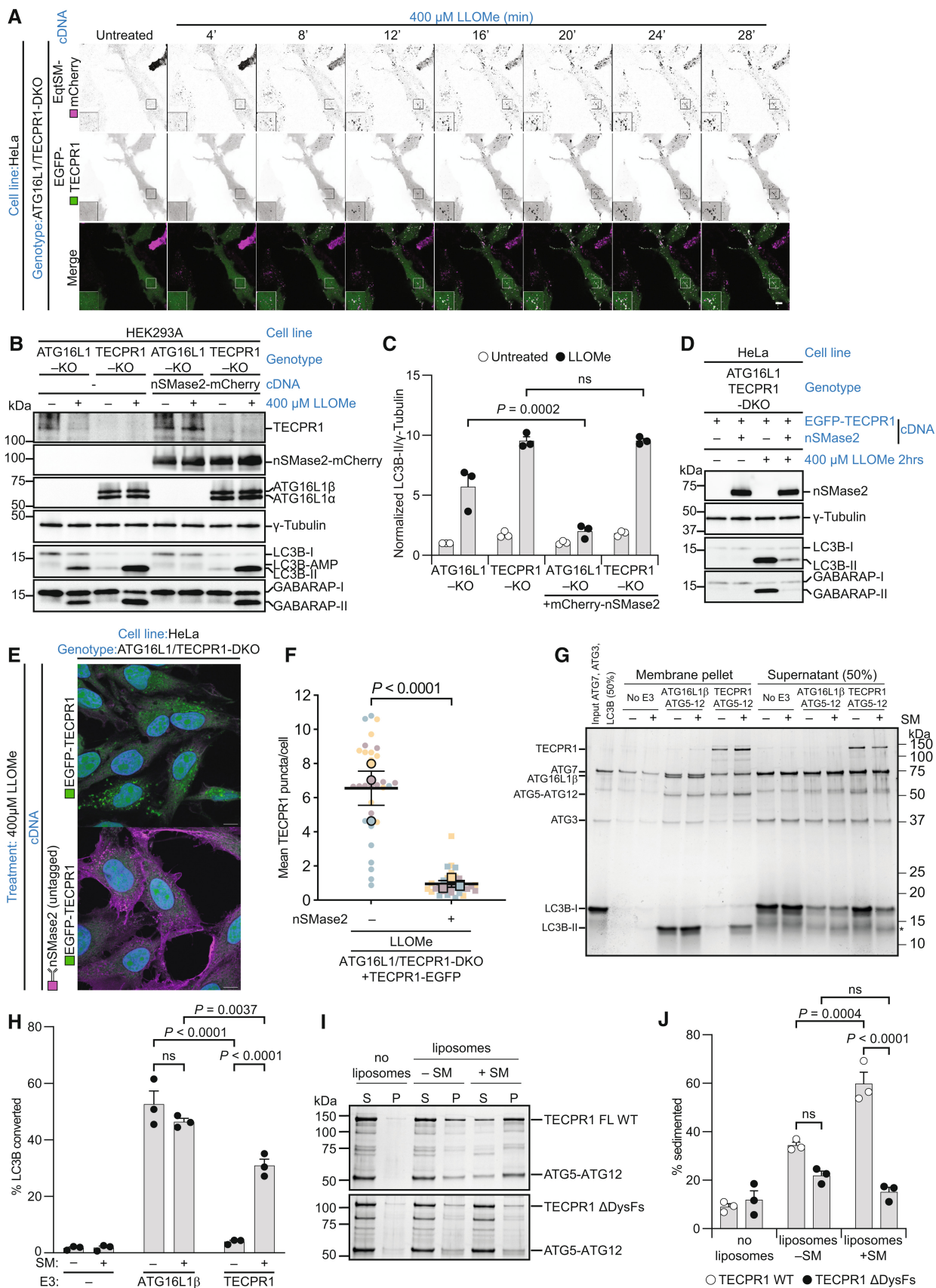
Figure 3.

cells in response to LLOMe treatment (Fig EV5B), mNeonGreen-TECPR1 puncta formed to the same extent in both WT and PI4K2A-KO cells (Fig EV5C and D). Together, our data show that TECPR1 is recruited to PtdIns4P and SM-positive compartments, but whereas PtdIns4P is dispensable, SM is essential for TECPR1 recruitment.

Dysferlin domains are essential for TECPR1 recruitment and activity at damaged lysosomes

Based on a structural prediction by AlphaFold (Jumper et al, 2021; Varadi et al, 2022), the two DysF domains of TECPR1, denoted DysF1 and DysF2, protrude from each of the two tectonin propellers (Fig 4A and B). A surface representation of the two DysF domains with lipophilicity mapping showed a few hydrophobic amino acids at the tip of each DysF domain (Fig 4B). We therefore decided to mutate amino acids on the hydrophobic surfaces in DysF1 (W77A or W154A) and DysF2 (W829A or W908A) to analyze their effect on TECPR1-mediated LC3B and GABARAP lipidation. To this end, ATG16L1/TECPR1-DKO HEK293A cells were rescued with WT or mutant TECPR1 and treated with LLOMe to induce ATG8ylation. Indeed, all four DysF mutations greatly inhibited ATG8ylation, with W77A (DysF1) and W829A (DysF2) showing the largest decrease in LC3B and GABARAP lipidation (Fig 4C and D). When ATG16L1/TECPR1-DKO cells were transduced with a double mutant (TECPR1 W77A/W829A, hereafter referred to as WAWA), LC3B and GABARAP lipidation in response to LLOMe was completely abolished without affecting the protein stability of TECPR1 (Fig 4E and F). In line with this, the EGFP-TECPR1 WAWA mutant was not recruited to puncta in LLOMe-treated cells, contrary to WT TECPR1 (Fig 4G and H). Thus, our data indicate that both DysF domains of TECPR1 are essential for its recruitment to damaged lysosomes and for its E3-like function in ATG8ylation.

Dysferlin domains mediate SM-binding and activation of TECPR1 in vitro

To further elucidate the importance of the DysF domains, we analyzed the activities of wild-type and DysF mutant TECPR1 in the in vitro LC3 lipidation assay. Consistent with the results obtained in cells, deletion of either DysF domain of TECPR1 (ΔDysF1 or ΔDysF2) caused a dramatic loss of LC3B lipidation to liposomes containing SM (Fig 5A and B), indicating that the two domains work together as a unit or together provide increased membrane avidity. In line with this, using the WAWA mutant of TECPR1 demonstrated that a single point mutation in each of the DysF domains was sufficient to eliminate SM specificity and significantly reduce liposome binding as confirmed by a co-sedimentation assay and liposome floatation assay (Fig 5C and D, Appendix Fig S2A and B). These findings reinforce the importance of DysF domains as sensors for SM. However, the isolated PH domain of TECPR1 bound strongly to liposomes regardless of whether SM was present in the liposomes (Fig 5E and F, Appendix Fig S2C and D), which may suggest that the membrane-binding activity of the PH domain is blocked in the native state of the TECPR1 structure and is available for binding only when DysF domains are engaged in SM binding. Such a mechanism would ensure that TECPR1-ATG5-ATG12 is active for lipidation only where SM is presented on the membrane.

TECPR1 rescues noncanonical autophagy blocked by Salmonella Typhimurium factor SopF

While ATG16L1 and TECPR1 seem redundant in CASM induced by several membrane-compromising agents, there are conditions where ATG16L1 activity is required while TECPR1 remains inactive, including treatment with ionophores like monensin and nigericin (Figs 1A and EV1A). Thus, we speculate that there might be an evolutionary advantage of having two distinct means to initiate CASM at compromised membrane compartments.

During infection, Salmonella Typhimurium secretes the T3SS effector SopF that targets the ATP6V0C subunit of the V-ATPase for riboxylation (Xu et al, 2019). This factor specifically blocks the interaction between ATG16L1 and the V-ATPase, and thus inhibits ATG16L1-mediated CASM. We therefore wondered whether SopF would also affect TECPR1 E3 activity or if TECPR1 could perform CASM when ATG16L1 is compromised. To test this, we generated HeLa cell lines (WT, ATG16L1-KO, TECPR1-KO, and DKO),

---

Figure 4. Dysferlin domains are essential for TECPR1 recruitment and activity at damaged lysosomes.

A   Schematic overview of TECPR1 domains and protein interaction sites, including Tectonin Repeats (TR, blue), Dysferlin domains (DysF, green), Disordered Region (DR, gray), ATG5 Interacting Region (AIR, orange) and Pleckstrin Homology domain (PH, pink).

B   Structural prediction of TECPR1 (UniProt Q7Z6L1) by AlphaFold, with the same coloring of domains as in (A). Each of the two Dysferlin domain surfaces was also mapped by lipophilicity, with dark cyan being the most hydrophilic and golden being the most lipophilic surfaces, and the residues W77, W154, W829, and F908 are outlined in red.

C   Immunoblot analysis of LC3B/GABARAP lipidation in ATG16L1-KO or ATG16L1/TECPR1-DKO HEK293A cells with or without rescue with TECPR1 (WT), TECPR1 W77A, TECPR1 W154A, TECPR1 W829A, or TECPR1 F908A, and treated with 400 μM LLOMe for 2 h. γ-Tubulin is a loading control.

D   Ratio of LC3B-II to γ-Tubulin quantified from immunoblots in (C) and normalized to ATG16L1-KO cells.

E   LC3B/GABARAP lipidation in ATG16L1/TECPR1-DKO HEK293A cells rescued with TECPR1 (WT), TECPR1 W77A, TECPR1 W829A, or TECPR1 W77A/W829A (WAWA), and treated with 400 μM LLOMe for 2 h. γ-Tubulin is a loading control.

F   Ratio of LC3B-II to γ-Tubulin quantified from immunoblots in (E) and normalized to cells rescued with TECPR1 (WT).

G   Maximum intensity projection of confocal images of HeLaK cells expressing EGFP-TECPR1 (WT) or W77A/W829A (WAWA) mutant, with or without 400 μM LLOMe for 30 min. Nuclei were counterstained with Hoechst 33342 (in blue). Scale bar: 10 μm

H   Beeswarm-Superplot displaying the mean number of EGFP-TECPR1 dots per cell per image of data represented in (G) quantified by automated analysis using CellProfiler. Mean ± SEM from each independent experiment (3/group) presented as large data points, with the black line corresponding to the mean of means. Individual data points (small) corresponding to single images are color-coded and superimposed according to the biological replicate they came from. Total cells per condition/images per condition: 2502/59 (WT untreated), 2549/48 (WT LLOMe), 2256/59 (WAWA untreated), and 2816/59 (WAWA LLOMe) were analyzed.

Data information: All data presented as mean + SEM (in (D) and (F)), n = 3 independent experiments. P-values determined using one-way ANOVA followed by Tukey's multiple comparisons test in (D), (F), and (H); ns = not significant.
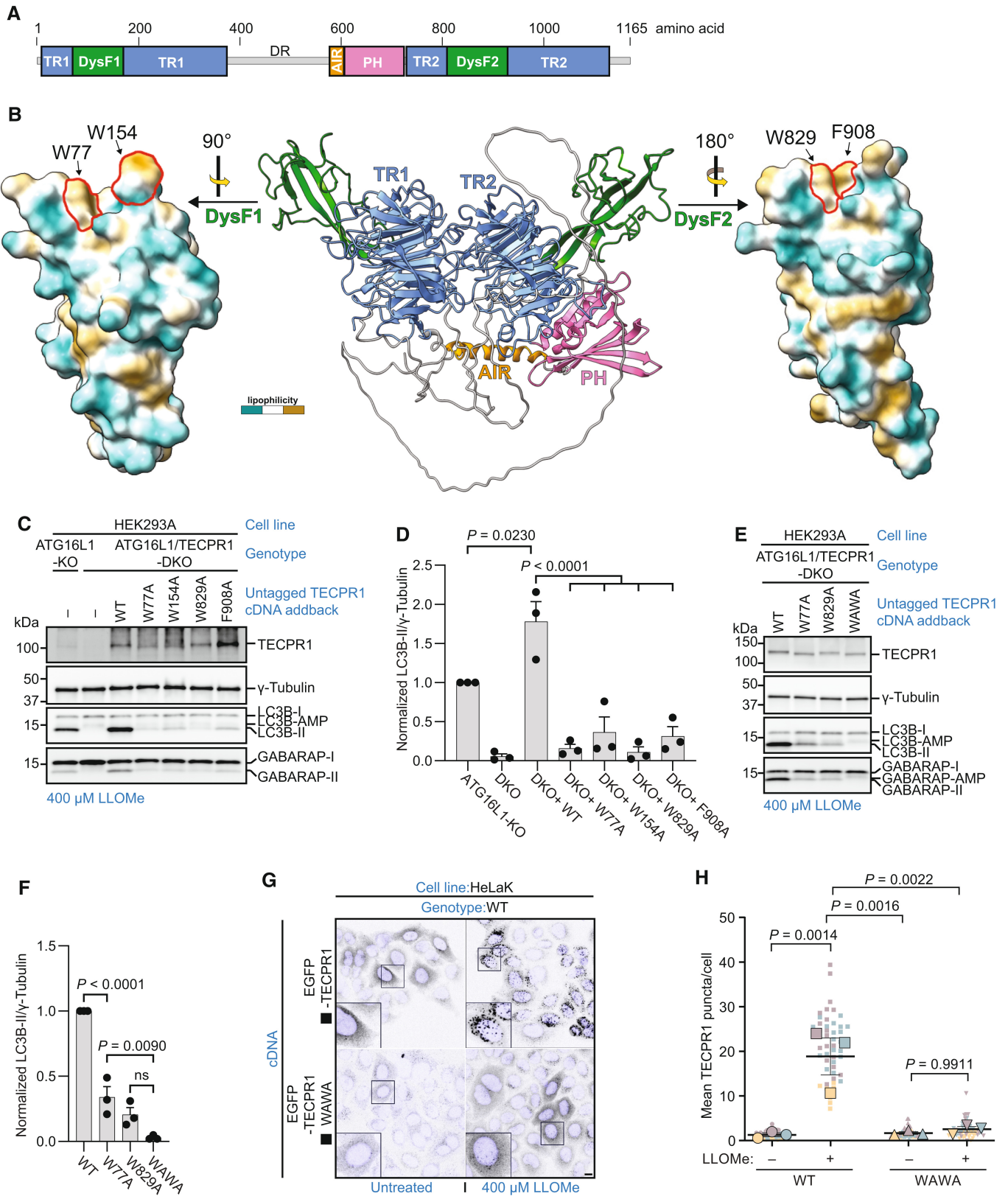
Figure 4.

expressing mCherry-SopF or not, and treated them with either monensin or LLOMe, along with ULK and VPS34 inhibitors to inhibit canonical autophagy. Monensin strongly induced LC3-lipidation in cells with ATG16L1 (WT and TECPR1-KO), but mCherry-SopF expression efficiently eliminated this response (Fig 6A and B). By contrast, we observed that TECPR1-expressing

cells (WT and ATG16L1-KO) were able to sustain ATG8 lipidation upon SopF expression after treatment with LLOMe, indicating that TECPR1 can facilitate CASM in response to membrane damage in the presence of SopF, counteracting *Salmonella* Typhimurium's immune evasion mechanism that targets ATG16L1 activity (Fig 6C and D). It should be noted that TECPR1's ATG8-lipidation activity is
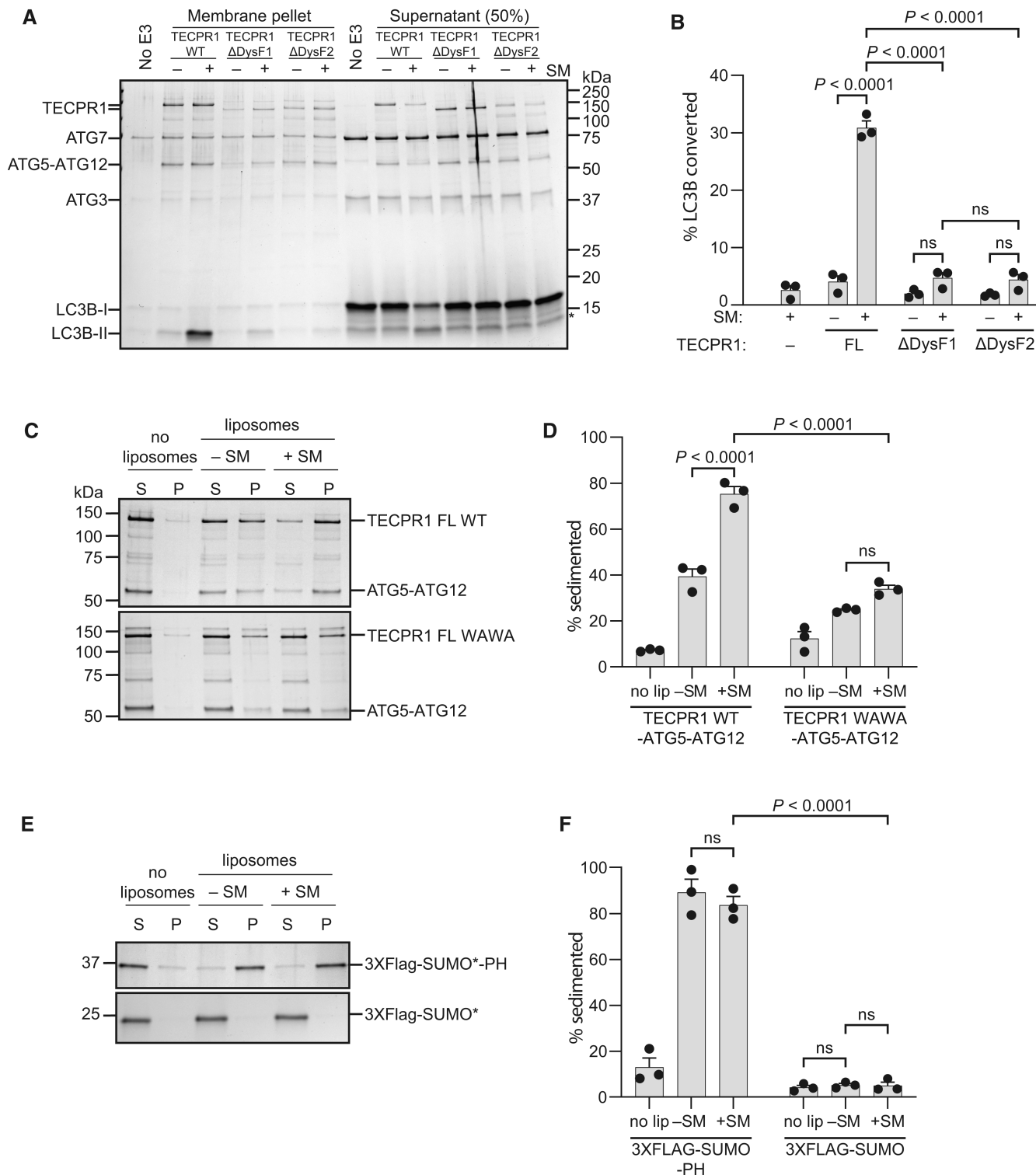

Figure 5.

Figure 5. Dysferlin domains mediate SM-binding and activation of TECPR1 *in vitro*.

A Coomassie-stained gel depicting *in vitro* LC3B lipidation reactions using the indicated combinations of proteins and liposomes (with or without SM), after being subjected to a liposome co-sedimentation assay. LC3B-AMP is denoted with an asterisk (*).

B The extent of LC3B-I to -II conversion in (A) was determined and plotted as percentage of total LC3B (Data presented as mean + SEM, *n* = 3 independent experiments, *P*-value from two-way ANOVA followed by Tukey's multiple comparisons test; ns = not significant).

C Liposome co-sedimentation assay of the indicated recombinant proteins and liposomes with or without SM. S, supernatant; P, pellet.

D Liposome binding in (C) was quantified as percentage of total protein in the pellet (Data presented as mean + SEM, *n* = 3 independent experiments, *P*-value from two-way ANOVA followed by Tukey's multiple comparisons test; ns = not significant).

E Liposome co-sedimentation assay of the indicated recombinant proteins and liposomes with or without SM. S, supernatant; P, pellet.

F Liposome binding in (C) was quantified as percentage of total protein in the pellet (Data presented as mean + SEM, *n* = 3 independent experiments, *P*-value from two-way ANOVA followed by Tukey's multiple comparisons test; ns = not significant).

more pronounced in ATG16L1-KO cells than in WT cells treated with SopF (Fig 6C and D). This suggests that the presence of inactive ATG16L1 may impact the availability of components required for TECPR1's activity, which is shared by both proteins.

To further support our findings, we conducted a microscopy analysis using WT and TECPR1-KO HeLa cells with or without stable expression of mCherry-SopF (Fig 6E and F). These cells were treated with the same combination of drugs and then analyzed for the presence of endogenous LC3B puncta. Indeed, TECPR1 was essential for the formation of LC3B-positive puncta and CASM in mCherry-SopF-positive cells (Fig 6E and F). Although TECPR1 was able to support LC3B-lipidation in the presence of SopF, the levels were significantly reduced due to the loss of ATG16L1 activity (Fig 6E and F). Additionally, we found that ATG16L1/TECPR1-DKO cells expressing EGFP-TECPR1 and mCherry-ATG16L1β with or without 2XFLAG-SopF lost puncta formation of mCherry-ATG16L1β, but not EGFP-TECPR1, upon expression of 2XFLAG-SopF after treatment with LLOMe (Appendix Fig S3A and B). Taken together, these experiments provide evidence for a critical role of TECPR1 in ATG8ylation following lysosomal damage in cells where ATG16L1 activity is blocked or not induced.

Discussion

Here we present direct evidence that TECPR1 forms a functional E3 complex for CASM together with ATG5-ATG12. Using combinations of KO cell lines and an *in vitro* assay we were able to demonstrate conditions where TECPR1 E3-activity is activated. Our findings further show that TECPR1 is kept inactive until it is exposed to

membrane damage. Detection of membrane damage is based on SM exposure on the target membrane, which is recognized by the DysF domains of TECPR1, and this interaction causes activation of the TECPR1 E3 complex (Fig 7). Indeed, both mutations and deletions of the DysF domains cause a complete loss of E3 functionality. Thus, exposed SM transmits danger signaling through TECPR1 and CASM. These findings are in complete accordance with the results and conclusions in an accompanying report (Boyle *et al*, 2023).

Diverse agents taken up by a cell produce different effects in the endolysosomal system, and a diversified and robust response to damage is critical for the maintenance of lysosome integrity. Reports indicate that parallel autophagy-related pathways contribute to the overall protection against harmful substances (Maejima *et al*, 2013; Durgan & Florey, 2022). ATG16L1-dependent CASM is established as an important pathway of defense that relies on the sensing of luminal ionic and pH imbalances, manifested by a structural change in the V-ATPase recruiting ATG16L1, a pathway called the V-ATPase-ATG16L1 axis (Xu *et al*, 2019). TECPR1-dependent CASM builds on another outcome of membrane damage, namely the exposure of SM to the cytosol. We denote this pathway as the SM-TECPR1 axis. As shown here, certain substances, such as LLOMe, can activate both pathways at the same time increasing the strength of defense. Certain stimuli are strong inducers of ATG16L1 activity but are unable to induce TECPR1-mediated LC3B/GABARAP lipidation. On the other hand, we show that SopF, which blocks ATG16L1 noncanonical autophagy activity, does not silence TECPR1 function. It is likely an advantage for a cell to have alternative activators of CASM as a broad defense against damage to intracellular membrane compartments and immune evasion.

ATG8 decoration of single membrane compartments of the endolysosomal network can serve multiple functions. Reports have

Figure 6. TECPR1 rescues CASM blocked by *Salmonella* Typhimurium factor SopF.

A LC3B/GABARAP lipidation in WT, ATG16L1/TECPR1-DKO, ATG16L1-KO, and TECPR1-KO HeLa cells with or without dox-inducible (2 μg/ml) expression of mCherry-SopF, treated as indicated for 2 h, were immunoblotted for the indicated proteins. γ-Tubulin is a loading control. MRT68921 and SAR405 are ULK and VPS34 inhibitors, respectively.

B Ratio of LC3B-II to γ-Tubulin or Vinculin quantified from immunoblots in (A) and normalized to WT monensin-treated cells (Data presented as mean + SEM, *n* = 3 independent experiments, *P*-value from two-way ANOVA followed by Tukey's multiple comparisons test; ns = not significant).

C LC3B/GABARAP lipidation in WT, ATG16L1/TECPR1-DKO, ATG16L1-KO, and TECPR1-KO HeLa cells with or without dox-inducible (2 μg/ml) expression of mCherry-SopF, treated as indicated for 2 h, Cell lysates were immunoblotted for the indicated proteins. γ-Tubulin is a loading control. MRT68921 and SAR405 are ULK and VPS34 inhibitors, respectively.

D Ratio of LC3B-II to γ-Tubulin or Vinculin quantified from immunoblots in (A) and normalized to WT monensin-treated cells (Data presented as mean + SEM, *n* = 3 independent experiments, *P*-value from two-way ANOVA followed by Tukey's multiple comparisons test; ns = not significant).

E Confocal images of WT and TECPR1-KO cells with or without dox-inducible (2 μg/ml) expression of mCherry-SopF, treated as indicated for 2 h. Nuclei were counterstained with Hoechst 33342 (in blue). Scale bar: 10 μm.

F Beeswarm-Superplot displaying number of LC3 puncta per cell in the images represented in (E) quantified by automated analysis using CellProfiler. Mean ± SEM from each independent experiment (3/group) presented as large data points, with the black line corresponding to the mean of means. Individual data points (small) corresponding to single cells are color-coded and superimposed according to the biological replicate they originated from. Total cells per condition/images per condition: 1169/30 (WT LLOMe), 1064/29 (WT-mcherry-SopF LLOMe), 692/23 (TECKO LLOMe), and 983/30 (TECKO-mcherry-SopF untreated) were analyzed (Data have skewed distribution. *P*-values were determined with Kruskal–Wallis followed by Dunn's multiple comparisons test).
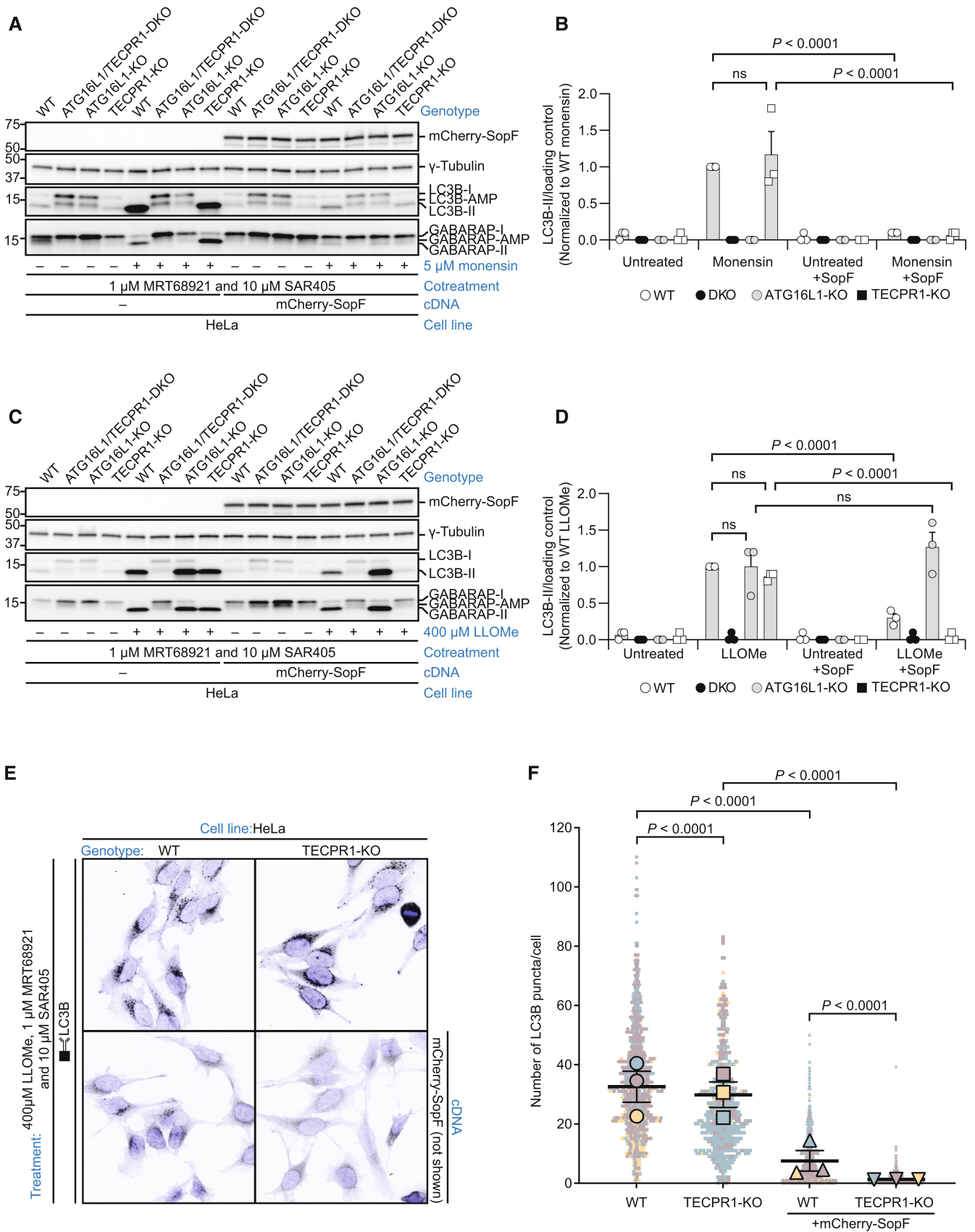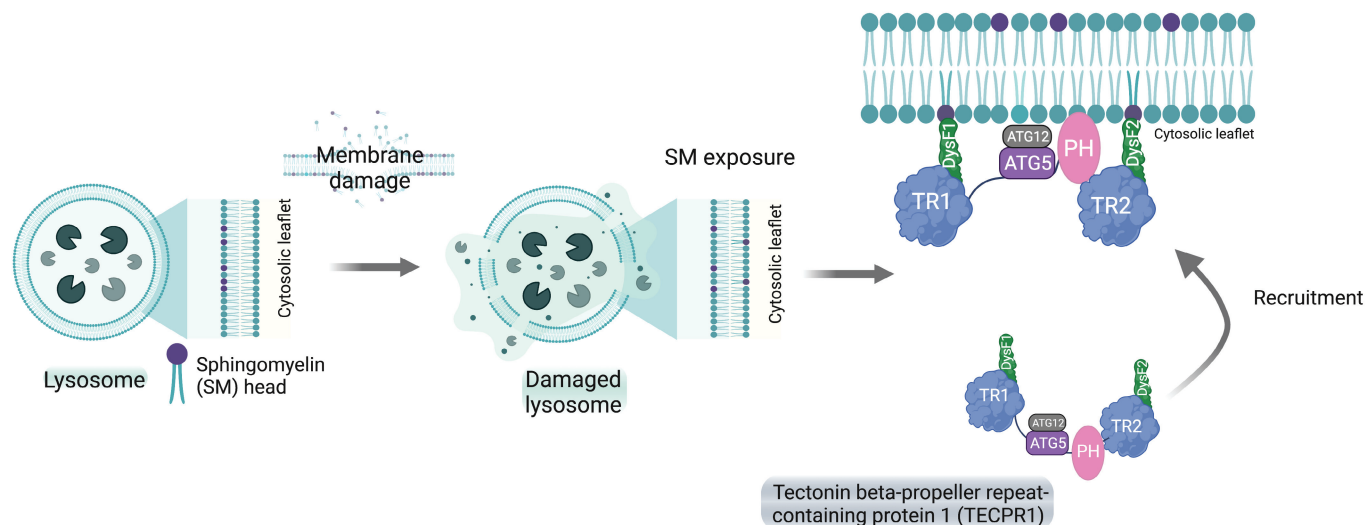
Figure 6.

Figure 7. Model for TECPR1 CASM activity.

Schematic representation of TECPR1 recruitment to the damaged membrane upon SM exposure. Created with Biorender.com.

argued that ATG8 proteins can modulate fusion and maturation events of the compartment they are attached to (Martinez et al, 2015; McEwan et al, 2015; Ligeon et al, 2021). Others have shown a role in signaling via the mTORC1 kinase complex and the transcription factor TFEB (Nakamura et al, 2020; Goodwin et al, 2021; Jia et al, 2022). Recently, the engagement of lipidated LC3A with ATG2 as an effector protein in CASM was reported (pre-print: Cross et al, 2023). However, the full effect of ATG8ylation on downstream events warrants further investigation.

Membrane repair processes are clearly beneficial for protection against invading pathogens (Boyle et al, 2023); however, we have demonstrated here that artificial delivery vehicles also can trigger a similar response. Endosomal escape is currently one of the most difficult barriers for efficient nucleotide delivery with LNPs. Current estimates are that only 1.5–3.5% of all internalized nucleotides achieve cytosolic delivery, hindering the progress and utilization of mRNA therapeutics (Gilleron et al, 2013; Wittrup et al, 2015). This TECPR1-mediated response may represent a novel target for improving LNP-mRNA delivery and a novel marker for endosomal disruption.

TECPR1 is a complex protein that takes part in the E3 reaction for ATG8ylation. We found that, normally, the protein is blocked in its activity and requires SM exposure on the target membrane to become active. The results shown in the present report clearly show that the two DysF domains play a crucial role in the recognition of SM. However, how SM binding is transmitted to the activation of TECPR1 is not clear. In a previous report (Lystad et al, 2019) we found that ATG16L1 requires an amphipathic helix (denoted helix 2) located next to the ATG5-interacting helix (helix 1) in order to bring the ATG5-ATG12 conjugate near the membrane, permitting ATG3-ATG8 to reach the co-substrate (PE/PS). Helix 2 consists of several hydrophobic amino acids situated on one side of the helix, which partly integrates into the membrane (Jensen et al, 2022). TECPR1 does not possess a similar structure or sequence near the ATG5-interacting helix (AIM). Instead, we propose that the role of

ATG16L1 helix 2 is harbored by the PH domain of TECPR1. This domain is more hydrophobic than most other members of the large family of PH domains, especially in its variable loop 1 region. We propose that a firm interaction with the membrane, through the partial insertion of hydrophobic amino acids, would allow a function of the PH domain similar to helix 2 of ATG16L1. The location of the PH domain next to AIM in TECPR1 is consistent with this hypothesis. The overall structure of TECPR1 therefore consists of at least three membrane-interacting domains: two DysF domains that sense SM and a PH domain that attaches the protein firmly to membranes via hydrophobic interactions. The membrane-binding activity of the PH domain must be inhibited in the absence of cytosolic SM, and there are several possibilities for how this can be achieved in this multidomain protein. Overall, the role of DysF domains would then be to recognize SM to open up the protein structure in order to allow membrane access of the PH domain.

DysF domains are found in several other metazoan proteins, among those the Ferlin family disease-related proteins Dysferlin and Myoferlin (Lek et al, 2010). DysF domains can take different forms and are sometimes duplicated and embedded at the protein level. However, very little is known about the specific function of any DysF domain. Here, we identify an SM-binding function when DysF domains are exposed on tectonin propeller structures. Intriguingly, it was recently reported that Myoferlin and Dysferlin can translocate from the plasma membrane to lysosomes to protect against damage induced by LLOMe (Gupta et al, 2021). It would be interesting to investigate whether other DysF-containing proteins also are engaged in the recognition of SM as a mechanism of membrane damage perception.

In summary, our results reveal that the novel CASM mediator and sphingomyelin-sensor, TECPR1, is activated by a wide range of pharmacological treatments, including clinically relevant lipid nano-particles, transfection reagents, antihistamines, lysosomotropic compounds, and detergents. Moreover, we reveal a complex damage-specific function for the distinct CASM machineries. Given the plethora of membrane damage-inducing agents, including mRNA

therapeutics, and subsequent activation of TECPR1, a meticulous investigation of its function is needed. Future studies aimed at better understanding both the structural and functional properties of TECPR1 can act as leverage to develop pathway or damage-specific therapies against pathogens or to improve endosomal escape strategies used in drug design to enhance intracellular delivery and efficacy.

Materials and Methods

Plasmid constructs

Plasmid constructs are listed in Table EV1 and construction details are available upon request. All plasmids were verified by DNA sequencing (Microsynth).

Cell culture

Human HEK293A, HeLa, and HeLa-Kyoto (HeLaK) cells were maintained in DMEM containing GlutaMAX, supplemented with 10% fetal bovine serum (FBS), 100 U/ml penicillin, and 100 μg/ml streptomycin. Cells were maintained at 37°C supplemented with 5% CO_2. The PC-3 ATG16L1-KO, ATG16L2-KO, TECPR1-KO, ATG16L1/ATG16L2-DKO, ATG16L1/TECPR1-DKO, and ATG16L1/ATG16L2/TECPR1-TKO cell lines were obtained from Shawn Bratton (The University of Texas, MD Anderson Cancer Center, USA). The PC-3 cells were cultured in DMEM/F-12 containing GlutaMax supplemented with 10% fetal bovine serum (FBS), 100 U/ml penicillin, and 100 μg/ml streptomycin, in a humidified 5% CO_2 atmosphere at 37°C.

Immunoblotting antibodies

ATG16L1 mouse mAb (MBL, M150-3, 1:1,000), ATG5 rabbit pAb (CST, 2630, 1:1,000), ATP6V0A2 rabbit pAb (Abcam, ab96803), GABARAP (E1J4E) rabbit mAb (CST, 13733, 1:1,000), γ-Tubulin (clone GTU-88) mouse mAb (Sigma-Aldrich, T6557, 1:10,000), GFP mouse mix of two monoclonal Ab (Roche, 11-814-460-001), LC3B (D11) XP rabbit mAb (CST, 3868, 1:1,000), mCherry goat pAb (Origene AB0040-200, 1:1,000), nsmase2 mouse pAb (Abcam, ab68735, 1:1,000), PI4K2A mouse mAb (Santa Cruz, sc-390026), TECPR1 (D6C10) rabbit mAb (CST, 8097, 1:1,000), Vinculin (clone hVIN-1) mouse mAb (Sigma-Aldrich, V9131, 1:3,000), HRP goat anti-mouse (Jackson ImmunoResearch, 115-035-003, 1:5,000), HRP donkey anti-goat (Jackson Immunoresearch, 115-035-004, 1:5,000) and HRP goat anti-rabbit (Jackson ImmunoResearch, 111-035-144, 1:5,000).

Immunofluorescence and antibodies

Cells seeded on coverslips were prepermeabilized or not, then fixed in 4% EM-grade formaldehyde in PHEM buffer (60 mM 1,4 piperazine diethylsulfonic acid (PIPES), 25 mM N-2-hydroxyethylpiperazine Nl-2-ethanesulfonic acid (HEPES), 10 mM EGTA, and 2 mM $MgC1_2$, pH 6.9) containing 5 μg/ml Hoechst 33342 for 30 min at room temperature (RT). Cells were washed twice in PHEM buffer containing 0.05% saponin to permeabilize the cells before staining with the indicated primary antibodies for 1 h at RT. Prior to staining with the secondary antibodies for 1 h at RT, cells were washed three times in PHEM buffer containing 0.05% saponin. Cells were mounted in ProLong Diamond antifade mountant. Prepermeabilization was performed on ice with 0.05% saponin in PEM buffer (80 mM K-Pipes, 5 mM EGTA, 1 mM MgCl2, pH 6.8) for 5 min.

Human anti-EEA1 serum 57 (IF 1:160,000) was a gift from Ban-Hock Toh, Melbourne, Australia (Mu et al, 1995), FLAG epitope M2 mouse mAb (Sigma F1804, 1:500), Galectin-3 goat pAb (R&D Systems, AF1154, 1:300), LAMP1 (clone H4A3) mouse mAb (H4A3 was deposited to the DSHB by August, J.T./Hildreth, J.E.K. (DSHB Hybridoma Product H4A3), 1:200), LC3B rabbit pAb (MBL, PM036, 1:500), nsmase2 mouse pAb (Abcam, ab68735, 1:200), SQSTM1 guinea pig pAb (Progen, GP62-C, 1:2,000), Ubiquitin (clone FK2) mouse mAb (Sigma-Aldrich, 04-263, 1:400), Alexa647 donkey anti-human (Jackson Immunoresearch, 709-605-149, 1:500), Alexa488 donkey anti-rabbit (Jackson ImmunoResearch, 711-545-152, 1:500), Alexa647 donkey anti-guinea pig (Jackson ImmunoResearch, 706-605-148, 1:500), Alexa647 donkey anti-mouse (Jackson ImmunoResearch, 715-605-150, 1:500) and Alexa647 donkey anti-goat (Jackson ImmunoResearch, 705-605-147, 1:500).

Reagents

Lipids used were 1-palmitoyl-2-oleoyl-sn-glycero-3-phosphocholine (POPC; Avanti Polar Lipids 850457C), 1,2-dioleoyl-sn-glycero-3-phosphoethanolamine (DOPE; Avanti Polar Lipids 850725C), 1-stearoyl-2-oleoyl-sn-glycero-3-phospho-L-serine (SOPS; Avanti Polar Lipids 840039C), 1,2-distearoyl-sn-glycero-3-phosphocholine (DSPC; Millipore LP-R4-076), N-(Methylpolyoxyethylene oxycarbonyl)-1,2-dimyristoyl-sn-glycero-3-phosphoethanolamine (DMPE-PEG2k; Nof America Corporation, PM-020CN), sphingomyelin (SM; Avanti Polar Lipids 860586P), cholesterol (in liposomes, Calbiochem, 228111), cholesterol (in LNPs, Sigma-Aldrich, C8667), and DLin-MC3-DMA (generated by chemical synthesis at AstraZeneca).

Other reagents used were 10k MWCO Slide-A-Lyzer G2 cassette (ThermoFisher Scientific, 87730), Adenosine-5′-triphosphate (Sigma-Aldrich, A2383) (ATP), Amicon Ultra 30K centrifugal filter (Millipore, UFC803096), Ammonium chloride (NH_4Cl), anti-Flag M2 affinity gel (Sigma-Aldrich, A2220), Any kD Mini-PROTEAN® TGX Precast Protein Gels 15-well (for coomassie stains) Bio-Rad, 4569036, astemizole (Sigma-Aldrich, A2861), bafilomycin A1 (AH diagnostics, BML-CM110) (BafA1), BalanCD HEK293 Feed (Irvine Scientific, 91166), BalanCD HEK293 Liquid (Irvine Scientific, 91165), blasticidine S (InvivoGen, ant-bl-1), Citrate Buffer pH 3.0 (TekNova, Q2445), CleanCap Cy5-EGFP-mRNA (TriLink, L7701), CleanCap EGFP-mRNA (TriLink, L7201), cOmplete ULTRA protease inhibitors (Roche, 5892791001), cOmplete Mini EDTA-free Protease Inhibitor Cocktail (Roche, 11836170001), Criterion 4–20% gradient 18-well Tris–HCl gels (Bio-Rad, 345-0034), DMEM with GlutaMAX (Gibco, 61965-026), DMEM/F-12 with Glutamax (Gibco, 31331-028), Doxycycline hyclate (Sigma-Aldrich, D9891), DTT (Sigma-Aldrich, D0632), fetal bovine serum (FBS) (Sigma-Aldrich, F7524), Flag peptide (Sigma F3290), FluoroBrite DMEM (Gibco, A1896701), Formaldehyde 16% EM grade (Polysciences, 18814), FuGENE HD (Promega, E2311), GFP-Trap Agarose (Chromotek, gta), Glutamine-S (Sigma, G8541), Glutathione Sepharose 4B (GE healthcare, 17-

0756-01), Gly-Phe beta-naphthylamide (Abcam, ab145914) (GPN), HEPES (Gibco, 15630-056), Hoechst 33342 (Invitrogen, H3570), JetMessenger (Polyplus, 101000056), Laemmli Sample Buffer (Bio-Rad, 1610747), L-leucyl-L-leucine methyl ester (Cayman Chemical, 16008), monensin sodium salt (Sigma-Aldrich, M5273), MRT68921 (Selleckchem, S7949), N-Ethylmaleimide (Sigma-Aldrich, E3876) (NEM), nigericin (Sigma-Aldrich, N7143), nonfat milk (Millipore, 70166), Nonidet P40 (Thermo Scientific, 28324), Nycodenz (Sigma-Aldrich, D2158), OptiPro SFM (GIBCO, 12309019), PBS (Gibco, 20012), PEI MAX (MW 40,000) (Polysciences, 24765), penicillin and streptomycin (Sigma-Aldrich, P4333), PhosSTOP (Roche, 4906837001), Pierce BCA assay (Thermo Scientific, 23227), ProLong Diamond antifade mountant (Invitrogen, P36961), puromycin dihydrochloride (Sigma-Aldrich, P7255), Quant-iT Ribogreen dye (Thermo Fisher Scientific, R11490), Saponin from quillaja bark (Sigma-Aldrich, S7900), SAR405 (Selleckchem, S7682), torin 1 (Tocris, 4247), Sephacryl S-300 (GE Healthcare, 17059910), Sodium dodecyl sulfate, SDS (Sigma-Aldrich, L4390), SUMOstar protease (Life Sensors, SP4110), Super PiggyBac Transposase Expression Vector (SBI Bioscience, PB210PA-1-SBI), SuperSignal West Dura Extended Duration Substrate (Thermo Scientific, 34076), TCEP (Tris (2-carboxyethyl)phosphine) (Thermo Scientific, 20491), TransBlot Turbo RTA Transfer Kit (Bio-Rad, 1704274), and X-tremeGene9 (Roche, 6365779001).

Production of stable lentiviral and retroviral transduced cell lines

Third-generation lentivirus were generated using procedures and plasmids as previously described (Campeau *et al*, 2009). Briefly, tagged fusions of transgenes were generated as Gateway ENTRY constructs using standard molecular biology techniques. From these vectors, lentiviral transfer vectors were generated by Gateway LR recombination into lentiviral destination vectors (Gateway-enabled vectors); pLenti6/UbC/V5-DEST (Invitrogen) in addition to pLenti-PGK-Puro-DEST (Addgene plasmid 19068, a gift from Eric Campeau & Paul Kaufman). VSV-G pseudotyped lentiviral particles were packaged using a third-generation packaging system (Addgene plasmids 12251, 12253, and 12259, a gift from Didier Trono). Cells were then transduced with low virus titers and stable expressing populations were generated by antibiotic selection.

Stable transgenesis of HeLa cells by piggyBac (PB) transposons

To generate cells stably expressing nSMase2, mCherry-nSMase2, mCherry-sopF, mCherry-EqtSM, 2XFLAG-SopF, pENTR-tagged transgene of interest was combined with PB-TA-ERP2 (Addgene plasmid 80477, a gift from Knut Woltjen) using LR clonase recombination, to make PB-TA-ERP2-transgene of interest. This was transfected together with Super PiggyBac Transposase Expression Vector into cells (indicated in corresponding figure legends) using FuGENE HD. PB transgenic cells were isolated using puromycin selection at 2 µg/ml.

Immunoprecipitation of V-ATPases

HEK293A cells were cultured in 10 cm plates until they reached 90% confluency. They were then transfected with 5 µg of pYMA3-SidK(aa1-278)-GFP plasmid using FugeneHD transfection reagent (Promega) according to the manufacturer's instructions. The next day, cells were treated with 400 µM LLOMe for 1 h, or left untreated as a control. Cells were then prepermeabilized for 5 min on ice using 0.05% Saponin to remove GFP-SidK not attached to membrane-embedded V-ATPase before harvesting the cells according to Chromotek guidelines. For immunoprecipitation from cell lysates, GFP-tagged SidK(aa1-278) was pulled down using GFP-Trap beads (Chromotek) following the manufacturer's protocol. The resulting immunoprecipitates, input, and flowthrough samples were separated by SDS–PAGE and analyzed by western blotting.

Formulation of MC3 LNPs and characterization

MC3 LNPs were formed by microfluidic mixing using a NanoAssemblr (Precision Nanosystems). Lipids were prepared in EtOH at a mol% ratio of 50:38.5:10:1.5 (DLin-MC3-DMA, Cholesterol, DSPC, DMPE-PEG2k). mRNA cargo (80% CleanCap EGFP-mRNA and 20% CleanCap Cy5-EGFP-mRNA, or particles containing only 100% CleanCap EGFP-mRNA) was prepared in 50 mM Citrate Buffer pH 3.0. Lipid:mRNA (w:w = 10:1, N:P = ~3:1) were mixed using a 3:1 (mRNA:Lipids) ratio at a flow rate of 12 ml/min. Nanoparticles were dialyzed using a 10 k MWCO Slide-A-Lyzer G2 cassette against 20 mM Tris–pH 7.4 overnight at 4°C. LNPs were collected and adjusted to 20 mM Tris–pH 7.4, 8% (w/v) Sucrose, passed through a 0.2 µm filter and concentrated by centrifugation at 3,000 *g*/4°C/20 min using an Amicon Ultra 30K centrifugal filter by > 3-fold. Concentrated LNPs were verified for size, mRNA concentration, and encapsulation before aliquoting and storage at −80°C.

LNP size (Diameter, Z-average) and polydispersity index (PDI) was determined by dynamic light scattering utilizing a Malvern Zetasizer (λ = 633 nm, scattering angle = 173°). Standard viscosity and refractive index values for pure water at 25°C, 0.8872 mPa, and 1.33, respectively, were used for data analysis within Zetasizer software (v7.12, Malvern).

Quant-iT Ribogreen dye was used according to the manufacturer's guidelines ± 1% Triton to ascertain encapsulated mRNA by comparison to a relevant mRNA standard curve.

LNPs utilized in this study are seen in Table EV2.

Prior to usage, LNPs were thawed and diluted to 0.1 mg/ml in PBS before treatment as noted in figure legends.

Protein purification

ATG16L1β-ATG5–ATG12 complex, ATG7, and ATG3 (human sequences) were produced in HEK-F suspension cells (Invitrogen) and purified as previously described (Lystad *et al*, 2019) with the exception that the GST and 3xFlag-SUMO* purification tags were switched between ATG16L1β and ATG12, as was the case for the TECPR1-ATG5-ATG12 construct described below. Human LC3A (amino acids 2–120), LC3B (amino acids 2–120), LC3C (amino acids 2–126), GABARAP, GABARAP-L1, and GABARAP-L2 (all three GABARAPs amino acids 1–116) were expressed as GST-fusion proteins and purified from *E. coli* as previously described for LC3B (Durgan *et al*, 2021). After HRV 3C protease cleavage, the purified products contained an extra Gly (LC3s) or Gly-Pro (GABARAPs) at the amino terminus.

Human TECPR1-ATG5–ATG12 complex was expressed and purified from HEK-F cells as follows: pCMV plasmids encoding

TECPR1 (amino acids 2–1,165) with GST and a HRV 3 C protease cleavage site at the amino terminus, ATG5, ATG12 with 3xFlag-SUMOstar at the amino terminus, and ATG10, were mixed in a weight ratio of 3:3:3:1. In a typical expression, a total of 330 μg plasmid was mixed with 990 μg of PEI MAX (MW 40,000) in 6 ml of OptiPro SFM and added to 150 ml of HEK-F cells at 2–2.5 × 10^6 cells/ml. Cells were grown for 3 days on a shaker (160 rpm) at 37°C with 8% CO2 in 4 mM glutamine-supplemented BalanCD HEK293 Liquid, with the addition of 5% BalanCD HEK293 Feed after 1 and 2 days. Cells were harvested by centrifugation at 350 *g* for 5 min, washed with 30-ml PBS, and the cell pellet was lysed with 22-ml PBS containing 1% Nonidet P40, 1 mM EDTA, and cOmplete ULTRA protease inhibitors. After 15-min incubation on ice, lysed cells were centrifuged at 350 *g* for 5 min and the supernatant was collected, snap-frozen in liquid nitrogen, and stored at −80°C. After thawing, the sample was centrifuged at 20,000 *g* for 10 min and the supernatant was added to 3-ml anti-FlagM2 affinity gel, and incubated overnight in the cold by end-to-end rotation. The gel matrix was transferred to a column and washed step-wise with 10 ml of NT350 (350 mM NaCl, 20 mM Tris–HCl, pH 7.4) containing 0.1% Nonidet P40 and 3 × 10 ml of NT350 without detergent. The gel was resuspended in 1-ml NT350 to which was added 2 μl SUMOstar protease and the closed column was incubated in the refrigerator overnight. Cleaved protein was eluted by step-wise 1-ml additions of NT350, and fractions with highest amount of protein were pooled. TCEP was added to 1 mM, and the mixture was added to 1 ml of Glutathione Sepharose 4b, equilibrated with NT350. After incubation overnight by end-to-end rotation in the cold, the gel matrix was washed three times with 10-ml NT350 and resuspended in 0.5-ml NT350 with 1 mM TCEP, and 16 μg GST-HRV 3 C protease was added (produced in-house at 4 mg/ml by expression from a pGEX plasmid in Escherichia coli). The gel was incubated in the refrigerator for 48 h, and the cleaved complex was collected, snap-frozen in liquid nitrogen, and stored at −80°C. All proteins in the complex had full-length authentic sequences, except TECPR1, which had Gly instead of Met at the amino terminus. Typical yield was 100–300 μg of complex from 150 ml of cell culture.

Complexes with TECPR1 lacking the first (ΔDysF1, deletion of amino acids Arg66-Arg168) or second (ΔDysF2, deletion of amino acids Thr814-Ser923), or both (ΔDysF1+2), DysF domain(s), and full-length complex with WAWA point mutations (Trp77Ala, Trp829Ala) in TECPR1 were purified using the same protocol as described above.

The PH domain of TECPR1 (amino acids 604–724), containing 3xFlag-SUMOstar at the amino terminus, was expressed in HEK-F cells and the lysate was prepared as described above. After binding to M2-agarose, the column was thoroughly washed with NT350 and eluted with 0.1 M Glycine-HCl pH 3.5. Protein fractions were pooled, TECP was added to 1 mM, and the material was gel filtrated on a 1 × 50 cm column of Sephacryl S-300 equilibrated with NT350. Fractions containing 3xFlag-SUMOstar-PH were pooled, concentrated to 2–4 μM, and stored in the freezer.

Liposome preparation

Liposomes (small unilamellar vesicles, SUVs) were prepared by mixing 150 μg POPC, 100 μg DOPE, 100 μg SOPS, 50 μg sphingomyelin, and 100 μg cholesterol, giving a composition of 30% POPC, 20% DOPE, 20% SOPS, 10% SM, and 20% cholesterol (w/w). For SUVs without SM, the amount of POPC was increased to 40%. Lipids were dried as a film from chloroform in flat-bottom glass tubes by evaporation with a fine stream of N2, followed by desiccation for 30 min at 50°C. Dried lipids were hydrated in 250 μl NT350 for 30 min at room temperature and vortexed (giving a total concentration of 2 mg lipid/ml). SUVs were made by sonication in a water bath at room temperature by 5-min pulses until the solution was essentially clear (1–3 pulses). Minor amounts of larger aggregates of material were removed by centrifugation at 200,000 *g* for 1 h and the supernatant was used immediately, or kept under N2 for up to 2 days in the refrigerator. Quality check was made by dynamic light scattering (Zetasizer Nano, Malvern Instruments) showing a mean diameter of approximately 50 nm for SUVs both with and without SM. SUVs lacking PS or PE, or both, were made by the same procedure and had lipid compositions as stated in Fig EV4.

In vitro LC3B-lipidation

To a total reaction volume of 40 μl in buffer, NT350 was added 0.4 μM ATG7, 0.5 μM ATG3, 5 μM ATG8, 1 mM ATP (containing 2 mM Mg^{2+}), 1 mM TCEP, and 1 mg/ml SUVs. When E3 complex was present, it was added to 0.2 μM (calculated as trimer for both ATG16L1β-ATG5–ATG12 and TECPR1-ATG5–ATG12). Incubation was done at 37°C for 1 h after which the samples were centrifuged at 50,000 rpm in a TLA-100 rotor (100,000 *g*$_{av}$) for 30 min (20°C) in order to separate liposome-bound (lipidated) ATG8-II in the pellet from soluble ATG8-I and ATG8-AMP adduct in the supernatant. The pellet was resuspended in 20 μl NT350 and equal volumes of pellet and supernatant were analyzed by SDS–PAGE and stained with coomassie brilliant blue.

Liposome co-sedimentation assay

Protein was mixed with liposomes (SUVs), or analyzed without the addition of liposomes, in a total volume of 40 μl in NT350, giving a final concentration of 0.5–1 μM protein and 1 mg/ml SUV. The mixture was incubated for 30 min at room temperature and centrifuged at 100,000 *g*$_{av}$ for 30 min (20°C). The pellet was resuspended in 40 μl NT350 and equal volumes of pellet, and the supernatant was analyzed by SDS–PAGE and stained with coomassie brilliant blue.

Liposome floatation assay

In 0.2-ml ultracentrifugation tubes (Beckman #343775), protein (1–2 μM) was mixed with 1 mg/ml liposomes (SUVs) in a total volume of 40 μl NT350. After incubation at room temperature for 30 min, 40 μl of 80% (w/v) of Nycodenz in NT350 was added and the samples were mixed by pipetting. On top was layered 80 μl of 30% (w/v) of Nycodenz in NT350, and a final layer of 40 μl NT350 was added. The samples were centrifuged at 100,000 rpm in a TLA-100 rotor (400,000 *g*$_{av}$) for 2 h at 20°C. The upper 100 μl was collected (Top fraction), and the remaining part was mixed by pipetting (Bottom fraction), analyzed by SDS–PAGE, and stained with coomassie brilliant blue together with an Input sample, after adjusting all samples to the same Nycodenz concentration.

Generation of knockout cells using CRISPR/Cas9

Knockout cells were generated using the pX459 system (Ran *et al*, 2013). In short, cells were transfected using X-tremeGene9 with pX459 vector (Addgene plasmid 62988, a gift from Feng Zhang) containing guides against ATG16L1, TECPR1, or ATG5. Twenty-four hours post-transfection, transfected cells were selected with 2 μg/ml puromycin for 72 h. The population of cells that survived selection was then seeded one cell per well in 96-well plates using a cell sorter (Sony SH800). The individual clones were expanded before knockouts were confirmed by western blotting or Sanger sequencing, primers to amplify the genomic target regions were adapted from a previously published study (Wible *et al*, 2019) and are included in Table EV3. Guide sequences for ATG5 and TECPR1 were also adapted from a previously published study (Wible *et al*, 2019), while the guide used for ATG16L1 was adapted from our previously published work (Lystad *et al*, 2019), guide sequences are included in Table EV4.

Western blotting

Cells were washed with PBS and lysed in Triton-lysis buffer (50 mM Tris–HCl pH 7.4, 150 mM NaCl, 1 mM EDTA, and 1% Triton-X 100) supplemented with protease and phosphatase inhibitor cocktails and 40 mM N-Ethylmaleimide, incubated at 4°C for 30 min with end-over-end rotation, before centrifugation at 21,000 *g* for 10 min at 4°C. Protein concentrations of cleared extracts were determined by the Pierce BCA assay and equalized with Triton-lysis buffer. Extracts were mixed with Laemmli Sample Buffer with DTT and incubated for 5 min at 95°C. Equal amounts of extracts (15 μg protein per lane) were loaded onto Criterion 4–20% gradient 18-well Tris–HCl gels and transferred to a LF PVDF, included in the RTA Transfer Kit, using a TransBlot® Turbo system. Membranes were blocked in 7.5% nonfat milk in PBS-Tween (0.05%) for 1 h at RT followed by incubation with primary antibodies in 5% BSA in PBS-Tween (0.05%) overnight at 4°C, followed by anti-rabbit- or anti-mouse-HRP in 5% nonfat milk in PBS-Tween (0.05%) for 1 h at RT. Band detection was performed with SuperSignal West Dura Extended Duration Substrate in an Azure Sapphire Biomolecular Imager. Quantification of WB data was performed with Azure Spot 2.1.097 software.

Microscopy

The fixed samples were imaged on a Nikon ECLIPSE Ti2-E inverted microscope (Nikon Corp, Tokyo, Japan) equipped with a CFI Plan Apo λ 40× (NA 0.95, Air) objective, CSU-W1 dual spinning disk (50 μm pinhole) confocal unit (Yokogawa Electric Corp, Tokyo, Japan), two Prime BSI sCMOS cameras (Teledyne Photometrics, Tucson, AZ, US), a laser unit with 405/488/561/638 nm lasers (120/100/100/100 mW), a multichannel LED light source (Lumencor SpectraX Chroma, Lumencor, OR, US) and with QUAD (DAPI/GFP/RFP/Af647) filter cubes for epifluorescence. Fig EV5 microscopy images were aquired with widefield fluorescence using Prime BSI A19M204025 camera a laser unit with 395/470 nm lasers and with QUAD (DAPI/GFP) filter cubes for epifluorescence. Images were exported to TIF in NIS-Elements AR Analysis software and processed into figure panels using the imageJ plugin FigureJ (Mutterer & Zinck, 2013). Image analysis was performed in CellProfiler (see below).

Live-cell confocal imaging was done with cells in a humidified chamber at 37°C supplemented with 5% CO2 on the Andor Dragonfly confocal spinning disk (Oxford Instrumentals) with a ×60 objective (NA 1.4) using a sCMOS (Zyla) camera. Here the cell medium was replaced with FluoroBrite DMEM supplemented with 10% fetal bovine serum (FBS), 2 mM Glutamine-S, 25 mM HEPES, 100 U/ml penicillin, and 100 μg/ml streptomycin before treatment, indicated in the figures, was added.

Multichannel images (DAPI/GFP/RFP/AF647 or DAPI/RFP/AF647) of 5–20 random fields of view (FOV) from each coverslip were captured. For each FOV, 7–11 sections were acquired (Z section spacing 0.5 μm). Images shown are either of a single plane or maximum intensity projections of Z-sections and were adjusted by linear brightness-contrast adjustments.

Image analysis

To determine the number of TECPR1 or LC3 puncta per cell, the identification and segmentation of nuclei, cells, and puncta were performed using CellProfiler 4.1.3 software (Stirling *et al*, 2021). Data were further analyzed using the shinyHTM web tool (Botelho *et al*, 2019). The representative panel images were processed and generated using ImageJ (Fiji) (Schindelin *et al*, 2012).

Statistics and reproducibility

The number of individual experiments and the number of cells analyzed are indicated in the figure legends. Data were analyzed for normal distribution using appropriate tests using GraphPad Prism version 9.1.0. If the data were normally distributed, parametric tests were used, and for skewed distribution, nonparametric tests were employed to measure statistical significance. The statistical tests performed for each experiment are specified in the figure legends. *P*-values are indicated for each experiment. In instances of multiple comparisons of means, we used one-way or two-way analysis of variance (ANOVA) followed by Tukey's to determine statistical significance, unless specified otherwise.

Data availability

Source data is deposited in BioStudies, accession number: S-BSST1091 (https://www.ebi.ac.uk/biostudies/studies/S-BSST1091).

Expanded View for this article is available online.

Author contributions

Namrita Kaur: Formal analysis; validation; investigation; visualization; methodology; writing – original draft; writing – review and editing. **Laura Rodriguez de la Ballina:** Formal analysis; investigation; writing – review and editing. **Håvard Styrkestad Haukaas:** Investigation; writing – review and editing. **Maria Lyngaas Torgersen:** Conceptualization; funding acquisition; investigation; methodology; writing – review and editing. **Maja Radulovic:** Investigation. **Michael J Munson:** Resources; writing – review and editing. **Alan Sabirsh:** Resources; writing – review and editing. **Harald Stenmark:** Resources; funding acquisition; writing – review and editing. **Anne Simonsen:** Resources; funding acquisition; writing – review and editing. **Sven R Carlsson:** Conceptualization; resources; formal analysis; funding acquisition; investigation; visualization; methodology; writing – original draft; writing – review and editing. **Alf Håkon Lystad:** Conceptualization; formal analysis; funding acquisition; investigation; visualization; methodology; writing – original draft; project administration; writing – review and editing.

Disclosure and competing interests statement

The authors declare the following competing interests: M.J.M and A.l.S. are employees of AstraZeneca. All other authors declare no competing interests.

References

Abbas YM, Wu D, Bueler SA, Robinson CV, Rubinstein JL (2020) Structure of V-ATPase from the mammalian brain. *Science* 367: 1240–1246

Akinc A, Maier MA, Manoharan M, Fitzgerald K, Jayaraman M, Barros S, Ansell S, Du X, Hope MJ, Madden TD *et al* (2019) The Onpattro story and the clinical translation of nanomedicines containing nucleic acid-based drugs. *Nat Nanotechnol* 14: 1084–1087

Botelho H, Tischer C, Halavatyi A, Amaral M, Pepperkok R (2019) shinyHTM - interactive high-throughput microscopy analysis. *Zenodo* https://doi.org/10.5281/zenodo.2594651

Boyle KB, Ellison CJ, Elliott PR, Schuschnig M, Grimes K, Dionne MS, Sasakawa C, Munro S, Martens S, Randow F (2023) TECPR1 conjugates LC3 to damaged endomembranes upon detection of sphingomyelin exposure. *EMBO J* https://doi.org/10.15252/embj.2022113012

Campeau E, Ruhl VE, Rodier F, Smith CL, Rahmberg BL, Fuss JO, Campisi J, Yaswen P, Cooper PK, Kaufman PD (2009) A versatile viral system for expression and depletion of proteins in mammalian cells. *PLoS One* 4: e6529

Chen D, Fan W, Lu Y, Ding X, Chen S, Zhong Q (2012) A mammalian autophagosome maturation mechanism mediated by TECPR1 and the Atg12-Atg5 conjugate. *Mol Cell* 45: 629–641

Choy A, Dancourt J, Mugo B, O'Connor TJ, Isberg RR, Melia TJ, Roy CR (2012) The legionella effector RavZ inhibits host autophagy through irreversible Atg8 deconjugation. *Science* 338: 1072–1076

Cross J, Durgan J, McEwan DG, Florey O (2023) Lysosome damage triggers direct ATG8 conjugation and ATG2 engagement via CASM. *bioRxiv* https://doi.org/10.1101/2023.03.22.533754 [PREPRINT]

Dowdy SF (2017) Overcoming cellular barriers for RNA therapeutics. *Nat Biotechnol* 35: 222–229

Durgan J, Florey O (2022) Many roads lead to CASM: diverse stimuli of noncanonical autophagy share a unifying molecular mechanism. *Sci Adv* 8: eabo1274

Durgan J, Lystad AH, Sloan K, Carlsson SR, Wilson MI, Marcassa E, Ulferts R, Webster J, Lopez-Clavijo AF, Wakelam MJ *et al* (2021) Non-canonical autophagy drives alternative ATG8 conjugation to phosphatidylserine. *Mol Cell* 81: 2031–2040

Ellison CJ, Kukulski W, Boyle KB, Munro S, Randow F (2020) Transbilayer movement of sphingomyelin precedes catastrophic breakage of enterobacteria-containing vacuoles. *Curr Biol* 30: 2974–2983

Firestone RA, Pisano JM, Bonney RJ (1979) Lysosomotropic agents. 1. Synthesis and cytotoxic action of lysosomotropic detergents. *J Med Chem* 22: 1130–1133

Flavin WP, Bousset L, Green ZC, Chu Y, Skarpathiotis S, Chaney MJ, Kordower JH, Melki R, Campbell EM (2017) Endocytic vesicle rupture is a conserved mechanism of cellular invasion by amyloid proteins. *Acta Neuropathol* 134: 629–653

Fletcher K, Ulferts R, Jacquin E, Veith T, Gammoh N, Arasteh JM, Mayer U, Carding SR, Wileman T, Beale R *et al* (2018) The WD40 domain of ATG16L1 is required for its non-canonical role in lipidation of LC3 at single membranes. *EMBO J* 37: e97840

Fujita N, Itoh T, Omori H, Fukuda M, Noda T, Yoshimori T (2008) The Atg16L complex specifies the site of LC3 lipidation for membrane biogenesis in autophagy. *Mol Biol Cell* 19: 2092–2100

Gilleron J, Querbes W, Zeigerer A, Borodovsky A, Marsico G, Schubert U, Manygoats K, Seifert S, Andree C, Stoter M *et al* (2013) Image-based analysis of lipid nanoparticle-mediated siRNA delivery, intracellular trafficking and endosomal escape. *Nat Biotechnol* 31: 638–646

Goodwin JM, WGt W, Hooper K, Li T, Kishi-Itakura C, Ng A, Lehmberg T, Jha A, Kommineni S, Fletcher K *et al* (2021) GABARAP sequesters the FLCN-FNIP tumor suppressor complex to couple autophagy with lysosomal biogenesis. *Sci Adv* 7: eabj2485

Gupta S, Yano J, Mercier V, Htwe HH, Shin HR, Rademaker G, Cakir Z, Ituarte T, Wen KW, Kim GE *et al* (2021) Lysosomal retargeting of Myoferlin mitigates membrane stress to enable pancreatic cancer growth. *Nat Cell Biol* 23: 232–242

Hooper KM, Jacquin E, Li T, Goodwin JM, Brumell JH, Durgan J, Florey O (2022) V-ATPase is a universal regulator of LC3-associated phagocytosis and non-canonical autophagy. *J Cell Biol* 221: e202105112

Hou X, Zaks T, Langer R, Dong Y (2021) Lipid nanoparticles for mRNA delivery. *Nat Rev Mater* 6: 1–17

Ishibashi K, Fujita N, Kanno E, Omori H, Yoshimori T, Itoh T, Fukuda M (2011) Atg16L2, a novel isoform of mammalian Atg16L that is not essential for canonical autophagy despite forming an Atg12-5-16L2 complex. *Autophagy* 7: 1500–1513

Jackson LA, Anderson EJ, Rouphael NG, Roberts PC, Makhene M, Coler RN, McCullough MP, Chappell JD, Denison MR, Stevens LJ *et al* (2020) An mRNA vaccine against SARS-CoV-2 - preliminary report. *N Engl J Med* 383: 1920–1931

Jensen LE, Rao S, Schuschnig M, Cada AK, Martens S, Hummer G, Hurley JH (2022) Membrane curvature sensing and stabilization by the autophagic LC3 lipidation machinery. *Sci Adv* 8: eadd1436

Jia J, Wang F, Bhujabal Z, Peters R, Mudd M, Duque T, Allers L, Javed R, Salemi M, Behrends C *et al* (2022) Stress granules and mTOR are regulated by membrane atg8ylation during lysosomal damage. *J Cell Biol* 221: e202207091

Jumper J, Evans R, Pritzel A, Green T, Figurnov M, Ronneberger O, Tunyasuvunakool K, Bates R, Zidek A, Potapenko A *et al* (2021) Highly accurate protein structure prediction with AlphaFold. *Nature* 596: 583–589

Kim JH, Song HK (2015) Swapping of interaction partners with ATG5 for autophagosome maturation. *BMB Rep* 48: 129–130

Kumar S, Jia J, Deretic V (2021) Atg8ylation as a general membrane stress and remodeling response. *Cell Stress* 5: 128–142

Lek A, Lek M, North KN, Cooper ST (2010) Phylogenetic analysis of ferlin genes reveals ancient eukaryotic origins. *BMC Evol Biol* 10: 231

Ligeon LA, Pena-Francesch M, Vanoaica LD, Nunez NG, Talwar D, Dick TP, Munz C (2021) Oxidation inhibits autophagy protein deconjugation from phagosomes to sustain MHC class II restricted antigen presentation. *Nat Commun* 12: 1508

Lystad AH, Carlsson SR, de la Ballina LR, Kauffman KJ, Nag S, Yoshimori T, Melia TJ, Simonsen A (2019) Distinct functions of ATG16L1 isoforms in membrane binding and LC3B lipidation in autophagy-related processes. *Nat Cell Biol* 21: 372–383

Maejima I, Takahashi A, Omori H, Kimura T, Takabatake Y, Saitoh T, Yamamoto A, Hamasaki M, Noda T, Isaka Y *et al* (2013) Autophagy sequesters damaged lysosomes to control lysosomal biogenesis and kidney injury. *EMBO J* 32: 2336–2347

Martinez J, Malireddi RK, Lu Q, Cunha LD, Pelletier S, Gingras S, Orchard R, Guan JL, Tan H, Peng J *et al* (2015) Molecular characterization of LC3-associated phagocytosis reveals distinct roles for Rubicon, NOX2 and autophagy proteins. *Nat Cell Biol* 17: 893–906

Maruyama T, Noda NN (2021) Delineating the lipidated Atg8 structure for unveiling its hidden activity in autophagy. *Autophagy* 17: 3271–3272

McEwan DG, Popovic D, Gubas A, Terawaki S, Suzuki H, Stadel D, Coxon FP, Miranda de Stegmann D, Bhogaraju S, Maddi K *et al* (2015) PLEKHM1 regulates autophagosome-lysosome fusion through HOPS complex and LC3/GABARAP proteins. *Mol Cell* 57: 39–54

Mellouk N, Weiner A, Aulner N, Schmitt C, Elbaum M, Shorte SL, Danckaert A, Enninga J (2014) Shigella subverts the host recycling compartment to rupture its vacuole. *Cell Host Microbe* 16: 517–530

Mizushima N (2020) The ATG conjugation systems in autophagy. *Curr Opin Cell Biol* 63: 1–10

Mu FT, Callaghan JM, Steele-Mortimer O, Stenmark H, Parton RG, Campbell PL, McCluskey J, Yeo JP, Tock EP, Toh BH (1995) EEA1, an early endosome-associated protein. EEA1 is a conserved alpha-helical peripheral membrane protein flanked by cysteine "fingers" and contains a calmodulin-binding IQ motif. *J Biol Chem* 270: 13503–13511

Mulligan MJ, Lyke KE, Kitchin N, Absalon J, Gurtman A, Lockhart S, Neuzil K, Raabe V, Bailey R, Swanson KA *et al* (2020) Phase I/II study of COVID-19 RNA vaccine BNT162b1 in adults. *Nature* 586: 589–593

Mutterer J, Zinck E (2013) Quick-and-clean article figures with FigureJ. *J Microsc* 252: 89–91

Nakamura S, Shigeyama S, Minami S, Shima T, Akayama S, Matsuda T, Esposito A, Napolitano G, Kuma A, Namba-Hamano T *et al* (2020) LC3 lipidation is essential for TFEB activation during the lysosomal damage response to kidney injury. *Nat Cell Biol* 22: 1252–1263

Niekamp P, Scharte F, Sokoya T, Vittadello L, Kim Y, Deng Y, Sudhoff E, Hilderink A, Imlau M, Clarke CJ *et al* (2022) Ca^{2+}-activated sphingomyelin scrambling and turnover mediate ESCRT-independent lysosomal repair. *Nat Commun* 13: 1875

Ogawa M, Yoshikawa Y, Kobayashi T, Mimuro H, Fukumatsu M, Kiga K, Piao Z, Ashida H, Yoshida M, Kakuta S *et al* (2011) A Tecpr1-dependent selective autophagy pathway targets bacterial pathogens. *Cell Host Microbe* 9: 376–389

Radulovic M, Schink KO, Wenzel EM, Nahse V, Bongiovanni A, Lafont F, Stenmark H (2018) ESCRT-mediated lysosome repair precedes lysophagy and promotes cell survival. *EMBO J* 37: e99753

Radulovic M, Wenzel EM, Gilani S, Holland LK, Lystad AH, Phuyal S, Olkkonen VM, Brech A, Jaattela M, Maeda K *et al* (2022) Cholesterol transfer via endoplasmic reticulum contacts mediates lysosome damage repair. *EMBO J* 41: e112677

Ran FA, Hsu PD, Wright J, Agarwala V, Scott DA, Zhang F (2013) Genome engineering using the CRISPR-Cas9 system. *Nat Protoc* 8: 2281–2308

Runwal G, Stamatakou E, Siddiqi FH, Puri C, Zhu Y, Rubinsztein DC (2019) LC3-positive structures are prominent in autophagy-deficient cells. *Sci Rep* 9: 10147

Schindelin J, Arganda-Carreras I, Frise E, Kaynig V, Longair M, Pietzsch T, Preibisch S, Rueden C, Saalfeld S, Schmid B *et al* (2012) Fiji: an open-source platform for biological-image analysis. *Nat Methods* 9: 676–682

Shaughnessy LM, Hoppe AD, Christensen KA, Swanson JA (2006) Membrane perforations inhibit lysosome fusion by altering pH and calcium in Listeria monocytogenes vacuoles. *Cell Microbiol* 8: 781–792

Skowyra ML, Schlesinger PH, Naismith TV, Hanson PI (2018) Triggered recruitment of ESCRT machinery promotes endolysosomal repair. *Science* 360: eaar5078

Stirling DR, Swain-Bowden MJ, Lucas AM, Carpenter AE, Cimini BA, Goodman A (2021) CellProfiler 4: improvements in speed, utility and usability. *BMC Bioinformatics* 22: 433

Tan JX, Finkel T (2022) A phosphoinositide signalling pathway mediates rapid lysosomal repair. *Nature* 609: 815–821

Varadi M, Anyango S, Deshpande M, Nair S, Natassia C, Yordanova G, Yuan D, Stroe O, Wood G, Laydon A *et al* (2022) AlphaFold Protein Structure Database: massively expanding the structural coverage of protein-sequence space with high-accuracy models. *Nucleic Acids Res* 50: D439–D444

Wetzel L, Blanchard S, Rama S, Beier V, Kaufmann A, Wollert T (2020) TECPR1 promotes aggrephagy by direct recruitment of LC3C autophagosomes to lysosomes. *Nat Commun* 11: 2993

Wible DJ, Chao HP, Tang DG, Bratton SB (2019) ATG5 cancer mutations and alternative mRNA splicing reveal a conjugation switch that regulates ATG12-ATG5-ATG16L1 complex assembly and autophagy. *Cell Discov* 5: 42

Wittrup A, Ai A, Liu X, Hamar P, Trifonova R, Charisse K, Manoharan M, Kirchhausen T, Lieberman J (2015) Visualizing lipid-formulated siRNA release from endosomes and target gene knockdown. *Nat Biotechnol* 33: 870–876

Xu Y, Zhou P, Cheng S, Lu Q, Nowak K, Hopp AK, Li L, Shi X, Zhou Z, Gao W *et al* (2019) A bacterial effector reveals the V-ATPase-ATG16L1 Axis that initiates Xenophagy. *Cell* 178: e20

Yu Z, Li W, Brunk UT (2003) 3-Aminopropanal is a lysosomotropic aldehyde that causes oxidative stress and apoptosis by rupturing lysosomes. *APMIS* 111: 643–652

Zhen Y, Radulovic M, Vietri M, Stenmark H (2021) Sealing holes in cellular membranes. *EMBO J* 40: e106922